

Non-Abelian Vector Boson Dark Matter, its Unified Route and signatures at the LHC

Basabendu Barman,^{*} Subhaditya Bhattacharya,[†] and Sunando Kumar Patra[‡]

Department of Physics, Indian Institute of Technology Guwahati, North Guwahati, Assam- 781039, India

Joydeep Chakraborty[§]

Department of Physics, Indian Institute of Technology Kanpur, Kanpur, Uttar Pradesh- 208016, India

Vector boson dark matter (DM) appears in $SU(2)_N$ extension (N stands for neutral) of standard model (SM) where a global $U(1)_P$ symmetry breaks generalised lepton number $L = P + T_{3N}$ to $(-1)^L$ and stabilises the DM through modified R -parity. This model offers several novel features to study. For example, dominant t channel annihilation and dominant s channel direct search processes alongwith co-annihilation of the DM with the heavier gauge boson helps the DM achieve required relic density in a large region of parameter space evading present direct search bounds with a possibility of detection at XENON1T. On the other hand, the exotic particles of the model can be produced at the Large Hadron Collider (LHC) yielding multilepton final states. Hadronically quiet four lepton with large missing energy in specific can provide a smoking gun signature of such a framework. The model has a high scale motivation to be generated from a $E(6)$ gauge group. We study the details of $E(6) \rightarrow SM \otimes SU(2)_N$ breaking patterns (through D-parity odd/even cases) which yields important phenomenological consequences.

^{*} bb1988@iitg.ernet.in

[†] subhab@iitg.ernet.in

[‡] sunando.patra@gmail.com

[§] joydeep@iitk.ac.in

I. INTRODUCTION

The terrestrial astrophysical observations like rotation curve of spiral galaxies around the cluster [1, 2], inhomogeneity in cosmic microwave background radiation (CMBR) [3], or more recent observations in Bullet cluster [4] indicate towards the existence of dark matter (DM) in the universe. A particle description of DM is much sought after and a lot of efforts are made (for a brief review, see for example, [5, 6]) to accommodate it, in extensions of standard model (SM). A straightforward description of DM phenomenology occurs through thermal freeze out of weakly interacting massive particle (WIMP) (see for example, [7]) where excepting for the absence of electromagnetic charge, other properties of DM are less constrained. This yields a plethora of possibilities of DM model building, although an experimental verification is still awaited. For example, DM spin is completely unknown; hence DM can either be a scalar, fermion or a vector boson. Scalar (see for example, [8–12]) and fermionic (see for example, [13–20]) DMs can be realised with minimal extensions to SM and are discussed widely. However, vector boson DMs are rather difficult to come across because it requires an extension of the SM gauge group or even more exotic frameworks.

Abelian vector boson DM has been discussed in different contexts, for example in universal extra dimension models with conserved KK parity [21–23] or in little Higgs framework with T parity [24, 25] or in other $U(1)$ extensions of SM (for example, see [26, 27]). In this paper we have adjudged the possibility of having a non-abelian vector boson dark matter which arises in extension of SM by $SU(2)_N$ gauge group [28–31]. Subsequently $SU(2)_N$ is broken completely, yielding massive gauge bosons which are a function of $\{g_N, V_N\}$, where g_N is the $SU(2)_N$ gauge coupling and V_N is the $SU(2)_N$ breaking vacuum expectation value (VEV). This gauge group is dark in the sense that $SU(2)_N$ charges do not contribute to the hypercharge. Thus all three $SU(2)_N$ gauge bosons are electromagnetic charge neutral and the lightest one can in principle be a DM. The stability of the DM is ensured by an extra global symmetry $U(1)_P$, breaking of which explicitly breaks the generalised lepton number $L = P + T_{3N}$ to $(-1)^L$ and leads to a discrete R -charge as in supersymmetric theory. One of the main motivations of such a framework is to envisage an unified theory, $E(6)$ as we demonstrate, which subsequently breaks to $SM \otimes SU(2)_N$. In the process of $E(6) \rightarrow SM \otimes SU(2)_N$, D-parity is broken in presence of a $SU(2)_N$ scalar triplet which allows g_N to be different from $SU(2)_L$ gauge coupling and serves as a parameter of the theory. VEV of this triplet scalar, which is actually a relic of the D-parity breaking higher dimensional spin-0 representation, breaks the degeneracy of the dark gauge bosons and ensures a single component DM. Absence of the $SU(2)_N$ triplet (D-parity even case) leads to a constrained degenerate DM scenario, which is not viable from direct search constraints. Intermediate symmetry breaking takes care of the fact that hypercharge is determined without $SU(2)_N$ contribution, ensuring charge neutrality of the $SU(2)_N$ gauge bosons. DMs in context of $SO(10)$ Grand Unified Theory (GUT) has also been discussed (see for example, [32, 33]), but mostly in context of scalar and fermion DMs.

Phenomenology of the non-abelian vector boson DM is a major motivation of the paper, which is discussed in details under the lamppost of relic density constraints from WMAP [34]/PLANCK data [35] and spin independent direct search bounds from LUX [36]. The relationship between the masses of the exotic particles and DM with $SU(2)_N$ coupling (g_N) is evaluated for correct relic density and direct search cross-sections. The model survives over a large region of parameter space thanks to the feature that DM annihilation and direct search channels are not entirely related. Co-annihilation with the heavier gauge boson also helps the DM to achieve required relic density, without affecting direct search, which also helps the model survive even beyond XENON1T. Extended gauge group necessitates the presence of exotic fermions which can be produced at the Large Hadron Collider (LHC). They subsequently decay to DM providing a variety of signatures of multilepton final states that can testify such a framework in near future runs of LHC. Two of the possible channels that are discussed in this draft are opposite sign dilepton and hadronically quiet four lepton with large missing energy. Hadronically quiet four lepton channel in particular is shown to be a smoking gun signal of such a framework. Most of these phenomena was not discussed in the earlier analysis of this model [30].

The paper is organised as follows: The model and basic formalism is discussed in Sec. II; DM phenomenology is discussed in Sec. III including relic density and direct search constraints; in Sec. IV, we study unified framework under E_6 and subsequent constraints on the model parameters. Some benchmark points have been identified thereafter which are studied for collider signatures in Sec. V. We finally conclude in Sec. VI.

II. DARK VECTOR MULTIPLY AND EXOTIC PARTICLES

We consider an extension of SM by non-Abelian gauge symmetry, $SU(2)_N$ so that the theory under consideration is $SU(2)_N \otimes SU(2)_L \otimes U(1)_Y \otimes SU(3)_C$ gauge symmetric. Once the $SU(2)_N$ symmetry is broken, three gauge bosons under $SU(2)_N$ become massive. The lightest of them is considered as dark matter candidate of the model, having mass around TeV scale. Such a framework has already been proposed in [29, 30] and we adopt the same particle configuration. However, instead of restricting only to the low scale framework, we have embedded this model

in a high-scale unified framework which has been discussed in detail later. Apart from the aforementioned gauge symmetries of the model, a global abelian symmetry $U(1)_P$ has been introduced. This redefines the lepton number of the particles as $L = P + T_{3N}$. Explicit breaking of $U(1)_P$ breaks L to $(-1)^L$ and results in conservation of a discrete symmetry $R = (-1)^{3B+L+2J}$ (very similar to R-parity in supersymmetry), which stabilizes the lightest particle odd under R -parity and serves as DM. $SU(2)_N$ charges do not contribute to the hypercharge and thus to electromagnetic charge which is defined as $Q = T_{3L} + Y$. Hence, $X_{1,2,3}$ gauge bosons are electromagnetic charge neutral and the lightest vector boson (X_1) aptly fits into the criterion of a DM.

The particle content and their quantum numbers under $SU(2)_L \otimes SU(2)_N \otimes U(1)_Y \otimes SU(3)_C \otimes U(1)_P$ as suggested in [30] are as follows:

Fermions:

$$\begin{pmatrix} u \\ d \end{pmatrix} = [2, 1, 1/6, 3; 0], \quad u^c = [1, 1, -2/3, \bar{3}, 0], \quad (h_q^c \ d^c) = [1, 2, 1/3, \bar{3}, -1/2], \quad h_q = [1, 1, -1/3, 3, 1],$$

$$\begin{pmatrix} N \\ \nu \\ E \\ e \end{pmatrix} = [2, 2, -1/2, 1, 1/2], \quad (E^c \ N^c) = [2, 1, 1/2, 1, 0], \quad e^c = [1, 1, 1, 1, -1], \quad (\nu^c \ n^c) = [1, 2, 0, 1, -1/2],$$

Scalars:

$$\begin{pmatrix} \phi_1^0 & \phi_3^0 \\ \phi_1^- & \phi_3^- \end{pmatrix} = [2, 2, -1/2, 1, 1/2], \quad (\chi_1^0 \ \chi_2^0) = [1, 2, 0, 1, -1/2], \quad \begin{pmatrix} \phi_2^+ \\ \phi_2^0 \end{pmatrix} = [2, 1, 1/2, 1, 0],$$

$$\begin{pmatrix} \Delta_2^0/\sqrt{2} & \Delta_3^0 \\ \Delta_1^0 & -\Delta_2^0/\sqrt{2} \end{pmatrix} = [1, 3, 0, 1, 1].$$

The vertical parentheses indicate doublet under $SU(2)_L$ and the horizontal ones indicate doublet under $SU(2)_N$. For brevity, we just mention one family of the particle spectrum and assume that gauge and Yukawa interactions are flavour diagonal as they do not lead to an alternation to the phenomenology discussed here. The $SU(2)_N$ gauge bosons, namely $X_{1,2,3}$, are not assigned any global charge, as they are transforming as adjoint representation. Their respective T_{3N} quantum numbers are $[1, 0, -1]$. Thus the R-charge for $X_{1,2}$ is odd (-1) while that for X_3 is even (1), since $J = 1$ for them. The odd R-charged dark gauge bosons are stable as they cannot decay to a pair of SM particles or to other exotic particles as those are assumed heavier¹. Thus in our scenario, the lightest of $X_{1,2}$ qualifies to be DM candidate and in case of a degeneracy they may serve as degenerate DM scenario. Scalar potential of the model and the allowed Yukawa couplings are discussed in Appendix A and Appendix B respectively.

III. VECTOR BOSON AS DARK MATTER

In this section we will detail how the lightest $SU(2)_N$ gauge boson qualify as DM in terms of the parameters involved in the theory. In our scenario, following neutral scalars acquire VEV: $\chi_{1,2}^0, \phi_{1,2}^0, \Delta_{1,3}^0$. The $SU(2)_N$ and electro-weak symmetries are spontaneously broken through the VEV of χ_2^0 (κ_2) and $\phi_{1,2}^0$ ($v_{1,2}$) respectively. Due to the presence of a bi-doublet and a $SU(2)_L$ Higgs doublet, the physical Higgs field (h) can be written as a linear combination of CP-even neutral components ($\phi_{1,2}$) as $h = (v_1 h_1 + v_2 h_2)/v$ where $v = \sqrt{v_1^2 + v_2^2} = 246$ GeV, i.e., electro-weak symmetry breaking scale. The model behaves similar to a two Higgs doublet model of type II [37, 38], where part of the bi doublet $\begin{pmatrix} \phi_1^0 \\ \phi_1^- \end{pmatrix}$ couples to up type quarks and $\begin{pmatrix} \phi_2^+ \\ \phi_2^0 \end{pmatrix}$ couples to down type quarks. The full scalar potential of the model can be found in [30], which we have mentioned in the appendix of this paper.

The VEV ($\delta_{1,2}$) of the triplet components $\Delta_{1,3}^0$ also contribute to the $SU(2)_N$ gauge boson masses and causes the mass splitting between two lighter dark gauge bosons as :

$$m_{X_{1,2}}^2 = \frac{1}{2} g_N^2 [\kappa_2^2 + v_1^2 + 2(\delta_1 \mp \delta_2)^2]. \quad (1)$$

Obviously, absence of the triplets $\delta_1 = \delta_2 = 0$ will make $X_{1,2}$ degenerate: $m_{X_1}^2 = m_{X_2}^2 = \frac{1}{2} g_N^2 [\kappa_2^2 + v_1^2]$. The other gauge boson X_3 (even under R) mixes with the usual SM neutral gauge boson Z through

¹ Other odd R -charged particles are not electromagnetic charge neutral and hence do not qualify as DM. See [30].

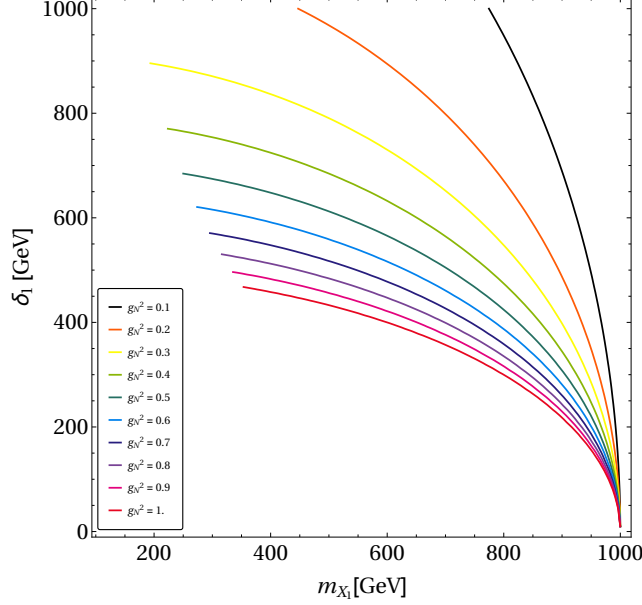


FIG. 1. Contours of triplet VEV δ_1 with DM mass m_{X_1} is shown for $m_{X_3} = 1$ TeV for different choices of $SU(2)_N$ coupling (g_N) in the maximum splitting scenario ($\delta_1 = \delta_2$). All the points below these lines are ruled out as they predict X_3 lighter than TeV.

$$m_{Z,X_3}^2 = \frac{1}{2} \begin{pmatrix} (g_1^2 + g_2^2) (v_1^2 + v_2^2) & -g_N \sqrt{g_1^2 + g_2^2} v_1^2 \\ -g_N \sqrt{g_1^2 + g_2^2} v_1^2 & g_N^2 [\kappa_2^2 + v_1^2 + 4(\delta_1^2 + \delta_2^2)] \end{pmatrix}. \quad (2)$$

The mass term for X_3 can be assumed as: $m_{X_3}^2 \approx \frac{1}{2} g_N^2 [\kappa_2^2 + v_1^2 + 4(\delta_1^2 + \delta_2^2)]$ as the $Z - X_3$ mixing is very much constrained [39]. Now from Eqn. (1), it is also evident that the maximum splitting between X_1 , X_2 can be achieved for $\delta_1 = \delta_2 = \delta$ where

$$m_{X_1}^2 = \frac{1}{2} g_N^2 [\kappa_2^2 + v_1^2]; \quad m_{X_2}^2 = m_{X_3}^2 = \frac{1}{2} g_N^2 [\kappa_2^2 + v_1^2 + 8\delta^2]. \quad (3)$$

In this framework, using the exclusion limit of $\sim \mathcal{O}(\text{TeV})$ from heavy neutral gauge boson search [40], we can put some lower limits on m_{X_1} depending on the choice of δ_1 . This is shown in Fig. 1 for the different values of $SU(2)_N$ gauge coupling (g_N) which we have used as a free parameter here. Each line indicates the minimum required m_{X_1} for a specific g_N . For example, with $g_N^2 = 0.4$ (light green line), m_{X_1} can be 400 GeV for large $\delta_1 \sim 750$ GeV. The smaller is the value of δ_1 , the larger is m_{X_1} which reaches the value of $m_{X_3} = 1$ TeV as the heavy gauge boson is degenerate to DM, $m_{X_3}^2 = m_{X_1}^2$ in the limit of $\delta_1 = \delta_2 = 0$ independent of the choice of g_N . Points above the contours are allowed as the X_3 masses become higher than 1 TeV, while the ones below yield lighter X_3 masses disfavoured by the data. Hence, this plot allows us to choose a minimum value for m_{X_1} as a function of δ_1 for a given g_N which will be used later for DM phenomenology. It is also quite apparent that the single component DM in this framework has to be X_1 as the lightest of the three neutral gauge bosons, in presence of the triplets $\delta_{1,2} \neq 0$. However, a more pathological situation arises when the triplet is absent or the vev is zero. The three of the gauge bosons are degenerate yielding a two component DM framework which necessarily requires to be heavier than ~ 1 TeV from the limit on m_{X_3} .

A. Relic Density and thermal freeze out of X_1

The fate of X_1 DM is primarily governed by the relic density requirement of the DM component in the universe. Now, $SU(2)_N$ gauge boson X_1 being odd under R-charge cannot directly couple to a pair of SM particles, but can

be connected to them through the exotic fermions (also odd under R) present in the theory. It is easy to identify the gauge couplings of X_1 from the structure of the particle multiplets presented in Sec. II. The $SU(2)_N$ gauge bosons will always connect the particle components in horizontal parenthesis, depicting $SU(2)_N$ doublets; for example, $\bar{d} h_q X_1$ or $\bar{E} e X_1$. Based on this, there are different channels through which X_1 can annihilate to SM particles which eventually help the DM to freeze out. Here, we have categorised them systematically:

- Annihilations to fermion pairs $d\bar{d}$; $e\bar{e}$; $\nu\bar{\nu}$ by exchanging h_q , E , N respectively,

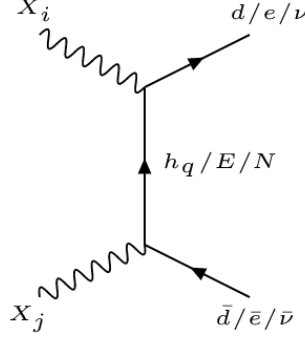


FIG. 2. Annihilations (Co-annihilations with $i \neq j$) to SM fermion pairs by exotic quark exchange.

- Annihilation to pair of Higgs by exchanging ϕ_3 , h and through four point contact term,

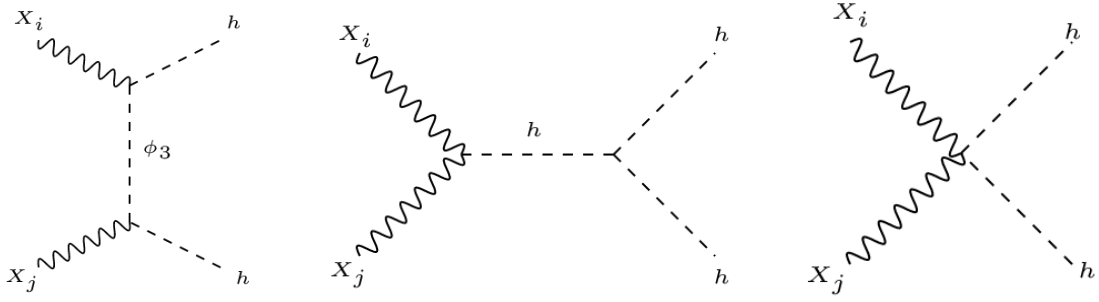


FIG. 3. Annihilations (Co-annihilations with $i \neq j$) to SM Higgs pair.

- Annihilation to pair of fermions and gauge bosons through Higgs exchange

It is easy to note that X_2 will have same channels to annihilate; but being heavier it will not be a DM. However, it can contribute to co-annihilation of X_1 , which will alter the relic density constraint of the model as we will discuss later. We would also like to note here that ϕ_3 exchange diagram is not going to contribute for the s -wave analysis, which we will perform here for calculation of relic abundance. s -wave contribution is obtained when the annihilation cross-sections are obtained at the threshold $s_0 = 4m_{X_1}^2$ and it will essentially not capture the temperature dependence terms. Then, $\langle\sigma v\rangle \sim \sigma v|_{s_0}$ and simplifies relic density calculation enormously. The justification of this approximation is very clear as all of the diagrams, except the mentioned one, will have non-zero s -wave contribution and the higher order terms are negligible. Now the total annihilation cross-section, computed from diagrams Figs. (2), (3) and (4),

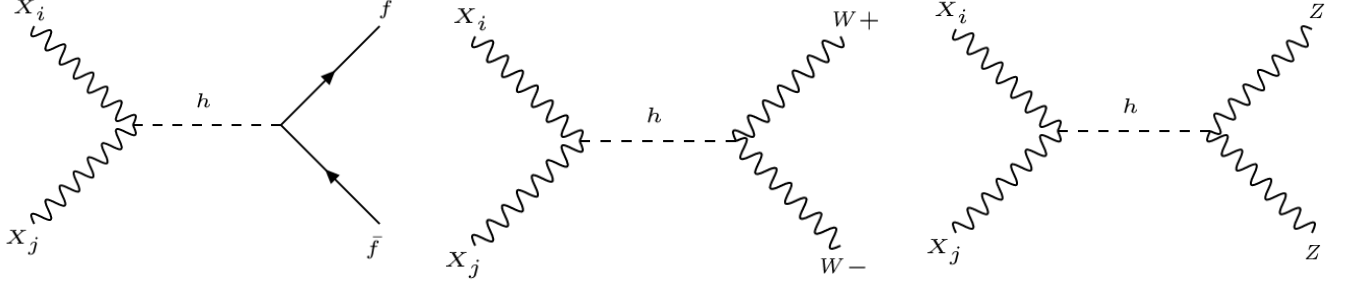


FIG. 4. Annihilations (Co-annihilations with $i \neq j$) to SM fermions and gauge bosons through Higgs exchange

can be written as [41]:

$$\begin{aligned}
 (\sigma v)_{X_1 X_1 \rightarrow \text{SM}}|_{s_0=4m_{X_1}^2} = & \frac{g_N^4 m_{X_1}^2}{72\pi} \left\{ \sum_{h_q} \frac{N_c}{(m_{h_q}^2 + m_{X_1}^2)^2} + \sum_E \frac{1}{(m_E^2 + m_X^2)^2} + \sum_N \frac{1}{(m_N^2 + m_{X_1}^2)^2} \right\} \\
 & + \frac{g_N^2}{2\pi} \left(\frac{v_1}{v} \right)^2 \left\{ \frac{1}{6} \frac{m_f^2}{(4m_{X_1}^2 - m_h^2)^2 + \Gamma_h^2 m_h^2} \left(1 - \frac{m_f^2}{m_{X_1}^2} \right)^{\frac{3}{2}} + \right. \\
 & \frac{1}{4m_{X_1}^2} \frac{m_Z^4}{(4m_{X_1}^2 - m_h^2)^2 + \Gamma_h^2 m_h^2} \left(1 - \frac{m_Z^2}{m_{X_1}^2} \right)^{\frac{1}{2}} + \\
 & \left. \frac{1}{4m_{X_1}^2} \frac{m_W^4}{(4m_{X_1}^2 - m_h^2)^2 + \Gamma_h^2 m_h^2} \left(1 - \frac{m_W^2}{m_{X_1}^2} \right)^{\frac{1}{2}} \right\} \\
 & + \frac{1}{32\pi m_{X_1}^2} \sqrt{1 - \frac{m_h^2}{m_{X_1}^2}} \left\{ \frac{1}{3} g_N^4 \left(\frac{v_1}{v} \right)^4 + \frac{3 g_N^2 m_h^4}{(4m_{X_1}^2 - m_h^2)^2 + \Gamma_h^2 m_h^2} \left(\frac{v_1}{v} \right)^2 + \right. \\
 & \left. \frac{2g_N^3 m_h^2 (4m_{X_1}^2 - m_h^2)}{(4m_{X_1}^2 - m_h^2)^2 + \Gamma_h^2 m_h^2} \left(\frac{v_1}{v} \right)^3 \right\}. \quad (4)
 \end{aligned}$$

Here, the first three terms in the above equation are the contributions from process given in Fig. 2. $N_c = 3$ is the colour factor which appears for the colour fermion (h_q) exchange only. The next three terms, proportional to $(v_1/v)^2$, are collective contributions from Fig. 3 where X_1 is annihilated to a pair of light fermions, charged and neutral gauge bosons respectively. The last three terms are contributions from Fig. 3 where dark matter is annihilated to a pair of Higgs. We would like to mention that for Higgs final state we have also included the interference contribution, see term proportional to $(v_1/v)^3$, which hardly contributes to the total annihilation. Higgs exchange diagrams are also suppressed by $(v_1/v)^2$ with $v_1 \ll v$ to adjust $X_3 - Z$ mixing.

While computing the annihilation cross-section, the following parameters are not theoretically constrained - $SU(2)_N$ gauge coupling g_N , which is not equal to SM, $SU(2)_L$ coupling for D-parity non-conserving scenario, and the masses of the exotic non-SM particles - yielding an effective six dimensional parameter space of the model as:

$$\{g_N, m_{X_1}, m_{h_q}, m_E, m_N, m_{\phi_3}\}. \quad (5)$$

It is easily appreciated that a scan in six dimensional parameter space to find the allowed parameter space of the model is difficult. We will hence simplify the situation to some extent by assuming $m_E, m_N, m_{\phi_3} = m$ which will still retain the main phenomenological implications of the model. To analyse the contributions from different annihilation channels to relic density, we have adopted two scenarios: (i) exotic fermions are heavier than the dark matter by 100 GeV, i.e. their masses are parametrised as $(m_{X_1} + 100)$ GeV, (ii) the exotic fermions are very heavy irrespective of the mass of X_1 , and we have set them to 500 GeV. The total annihilation cross-section is plotted with respect to DM mass and the individual contributions are also shown in Fig. 5.

From both the plots in Fig. 5, it is clear that amongst all degenerate exotic fermions, the contribution from h_q exchange diagram is visibly large due to its colour interaction. In both the plots, there is significant enhancement

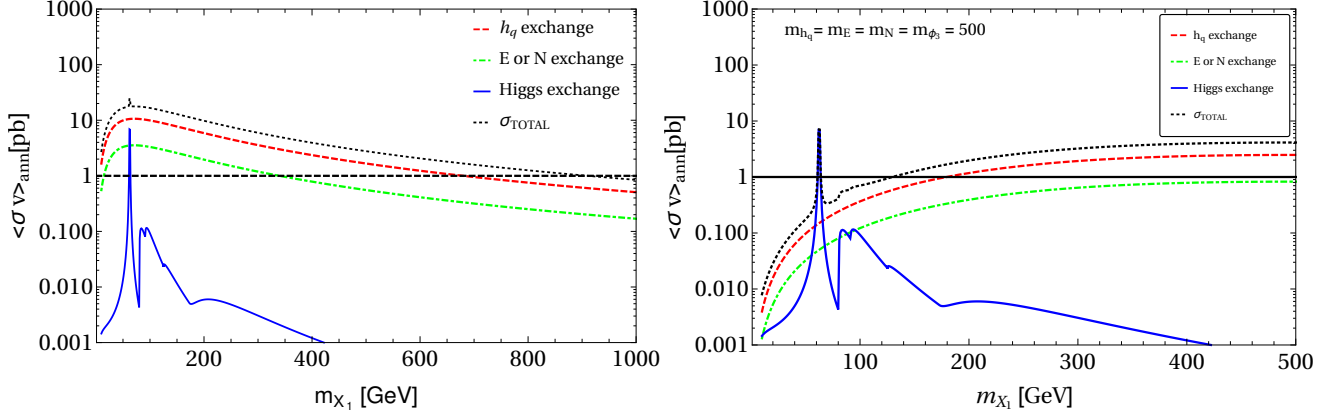


FIG. 5. Variations of total annihilation cross-sections $\langle \sigma v \rangle \sim \sigma v|_{s_0=4m_{X_1}^2}$ and contributions from different channels is shown as a function of DM mass (m_{X_1}) for two hypothesis: Left panel: mass of the exotic fermions are assumed to be ($m_{X_1} + 100$) GeV; Right panel: mass of the exotic fermions are fixed at 500 GeV. For both cases we set $g_N^2 = 0.4$ for illustration.

in the cross-section for Higgs exchange diagram at $m_{X_1} \simeq m_h/2$ for its resonance behaviour. There are relatively smaller peaks at $m_{X_1} \simeq m_W$ and $m_{X_1} \simeq m_Z$ as signatures of WW and ZZ final states.

The patterns of the individual contributions as well as the total annihilation cross-sections are different in left and right panels of Fig. 5. In the left panel, the exotic fermions are always 100 GeV heavier than the dark matter mass m_{X_1} , thus when the DM mass increases, the propagators become heavier which causes depletion in cross-section. In the right panel, the DM is lighter than the exotic fermions, but unlike the previous case, the propagator masses are fixed at 500 GeV. Thus, when m_{X_1} increases and approaches the masses of the exotic fermions, the availability of the final state phase space gradually increases, in turn eventually increasing the cross-section. It is worthy to note that in both the plots, the Higgs exchange diagram does not affect the total annihilation too much as it yields only a subdominant contribution through the powers of $\frac{v_1}{v}$ with $v_1 \ll v$ for satisfying the $Z - X_3$ mixing [39]. Horizontal black dotted lines denote the required annihilation cross-section to satisfy relic density constraints and the regions above it, with larger cross section under-closure (smaller density) while the regions below, with smaller cross-section, are ruled out by over closure (larger relic density).

We will now demonstrate the thermal freeze out of the vector boson DM (X_1) and eventually its relic density. To compute the thermal freeze out, we need to solve Boltzmann's equation [7] of the following form:

$$\dot{n}_{X_1} + 3Hn_{X_1} = -\langle \sigma v \rangle_{X_1 X_1 \rightarrow SM SM} \left[(n_{X_1})^2 - (n_{X_1}^{EQ})^2 \right], \quad (6)$$

where H is the Hubble constant and number density $n_{X_1}^{(EQ)}$ is given as:

$$n_{X_1}^{(EQ)} = \int \frac{\zeta_{X_1} d^3 p}{(2\pi)^3 2E} \tilde{f}_{X_1}^{(EQ)}, \quad \text{with equilibrium density } \tilde{f}_{X_1}^{EQ} = \frac{1}{e^{E/k_B T} - 1}. \quad (7)$$

In general $\langle \sigma v \rangle_{X_1 X_1 \rightarrow SM SM}$ is the thermal averaged cross-section defined as [7, 42]:

$$\langle \sigma v \rangle_{X_1 X_1 \rightarrow SM SM} = \int_{\hat{s}_0}^{\infty} d\hat{s} \frac{\zeta_{X_1}^2 \hat{s} \sqrt{\hat{s} - 4m_{X_1}^2} K_1(\frac{\sqrt{\hat{s}}}{T}) (\sigma v)_{X_1 X_1 \rightarrow SM SM}}{16 m_{X_1}^4 T K_2(\frac{m_{X_1}}{T})^2}, \quad (8)$$

where $K_{1,2}$ are the modified Bessel's functions, ζ_{X_1} is the internal degrees of freedom associated with X_1 , which is 3 for its vectorial nature, and $\hat{s} = (p_{X_1} + p'_{X_1})^2$. We will use the expression in Eq. 4, as well as the s -wave approximation to the thermal average cross-section as $\hat{s}_0 = 4m_{X_1}^2$, as has already been mentioned. With this approximation, Eq. 6 can be rewritten as:

$$\dot{n}_{X_1} + 3Hn_{X_1} = -(\sigma v)_{X_1 X_1 \rightarrow SM SM} \left[(n_{X_1})^2 - (n_{X_1}^{EQ})^2 \right]. \quad (9)$$

In order to identify the freeze-out of the DM, we will recast BEQ in terms of co-moving density (Y) as:

$$Y = \frac{n_{X_1}}{s}, \quad (10)$$

Here, the entropy density of the universe (s) is given by [7]

$$s = \frac{2\pi^2}{45} g_s(T) T^3; \quad \text{with } g_s(T) = r_k g_k \left(\frac{T_k}{T} \right)^3 \theta(T - m_k). \quad (11)$$

where the repeated index $k \in \{\text{all particles}\}$, is summed over. Here, T_k and g_k are the temperature and internal DOF of k^{th} particle with $r_k = 1$ (7/8) for boson(fermion).

Now we can rewrite Eq. 9 in terms of Y and $x = \frac{m_{X_1}}{T}$ as:

$$\frac{dY}{dx} = -\frac{x \langle \sigma v \rangle s}{H(m)} \left[(\sigma v)_{X_1 X_1 \rightarrow SM} (Y^2 - Y^{EQ^2}) \right], \quad (12)$$

where

$$H(m) = 1.66 \sqrt{g_*} \frac{m^2}{m_{Pl}}; \quad g_* = \sum_i \chi_i g_i \left(\frac{T_i}{T} \right)^4, \quad (13)$$

where i runs over bosons (fermions) with $\chi_i = 1$ (7/8) for bosons(fermions), and $m_{Pl} = \frac{1}{\sqrt{8\pi G}} = 2.43 \times 10^{18}$ GeV.

We also have the equilibrium co-moving number density

$$Y^{EQ} = 0.145 \frac{g}{g_{*s}} \left(\frac{m_{X_1}}{T} \right)^{\frac{3}{2}} e^{-\frac{m_{X_1}}{T}}. \quad (14)$$

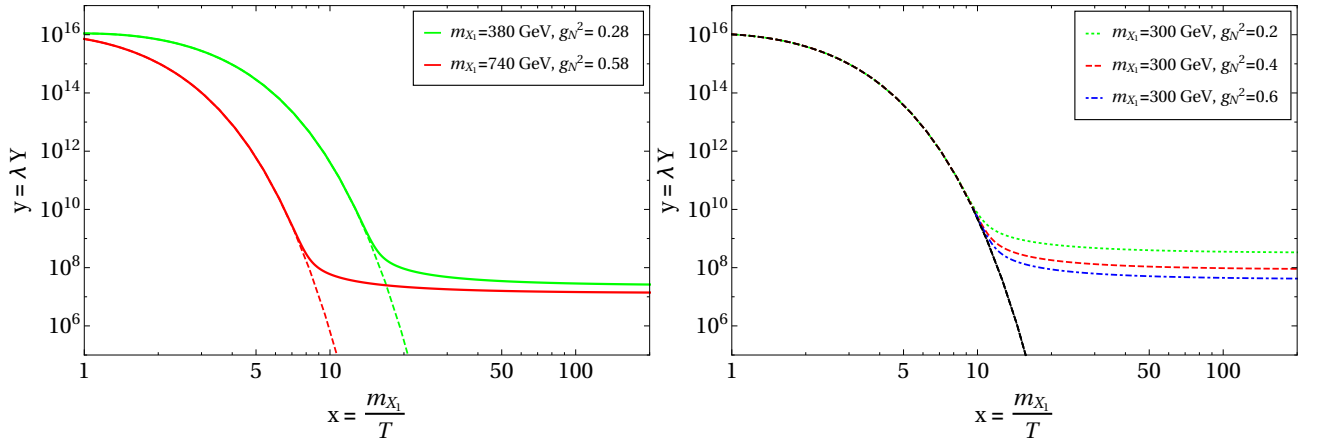


FIG. 6. Pattern of thermal freeze out of X_1 has been framed in $y = \lambda Y$ vs $x = m_{X_1}/T$ plane. Left-panel: $\{m_{X_1}, g_N\} = \{380 \text{ GeV}, 0.28\}, \{740 \text{ GeV}, 0.58\}$ are chosen as illustration. Dashed lines show the respective equilibrium distributions. Right-panel: different values of $g_N = \{0.2, 0.4, 0.6\}$ are chosen for same dark matter mass $m_{X_1} = 300 \text{ GeV}$.

Now the Boltzmann equation can be further simplified to a compact form as:

$$\frac{dy}{dx} = -\frac{m_{X_1}}{x^2} \left[\sigma_0 (y^2 - y^{EQ^2}) \right], \quad (15)$$

where $y = \lambda Y$ with $\lambda = (0.264 m_{Pl} \frac{g_{*s}}{\sqrt{g_*}})$, $\sigma_0 = (\sigma v)_{X_1 X_1 \rightarrow SM}$ given in Eq. 4.

We demonstrate the pattern of freeze out of the vector boson dark matter from equilibrium in Fig. 6. We have chosen two different sets of parameters for illustration: (i) Left panel of Fig. 6: two different combinations of $\{m_{X_1}, g_N\} = \{380 \text{ GeV}, 0.28\}, \{740 \text{ GeV}, 0.58\}$ are chosen and (ii) Right panel of the same figure: different values of $g_N = \{0.2, 0.4, 0.6\}$ are chosen for same dark matter mass $m_{X_1} = 300 \text{ GeV}$. Here, the dashed lines represent the corresponding equilibrium distributions. In the left plot, decoupling of green and red lines occur at $x = 20$ ($T \sim 19 \text{ GeV}$),

and $x = 7$ ($T \sim 105$ GeV) respectively. Due to different choices of the DM masses, the equilibrium distributions are different and the freeze out of the heavier component usually occurs early; but due to a very large coupling for the heavier component, the annihilation cross section is still larger for the heavier component than the lighter one and hence the yield is smaller for the heavier component. In the right panel, we show that the larger the coupling, the larger is the annihilation cross-section and the delay in the freeze out and smaller is the yield. Here, the freeze out occurs within $x = [10 : 15]$, depending on the coupling strength.

Relic density for a single component DM is related to the yield after freeze out as:

$$\Omega h^2 = \frac{m_{X_1} s_0 \sqrt{g_*}}{3H_0^2 m_{pl}^3 0.26g_{*s}} y(x_\infty), \quad (16)$$

where $y(x_\infty)$ is the solution of Eq. 15 at large values of x , and this can be written in terms of annihilation cross-section as:

$$\Omega h^2 \simeq \frac{2.4 \times 10^{-10} \text{GeV}^{-2}}{(\sigma v)_{X_1 X_1 \rightarrow SM SM}}. \quad (17)$$

Next we show the variation of relic density with DM mass in Fig. 7. The strategy of choosing other parameter remains the same as in Fig. 5. On the left hand side, we vary all the exotic fermion masses as $(m_{X_1} + 100)$ GeV while on the right hand side, we keep them fixed at 500 GeV and vary DM mass within that. In both the plots there is significant enhancement in the cross-section for Higgs exchange diagram at $m_{X_1} \simeq m_h/2$ for its resonance behaviour.

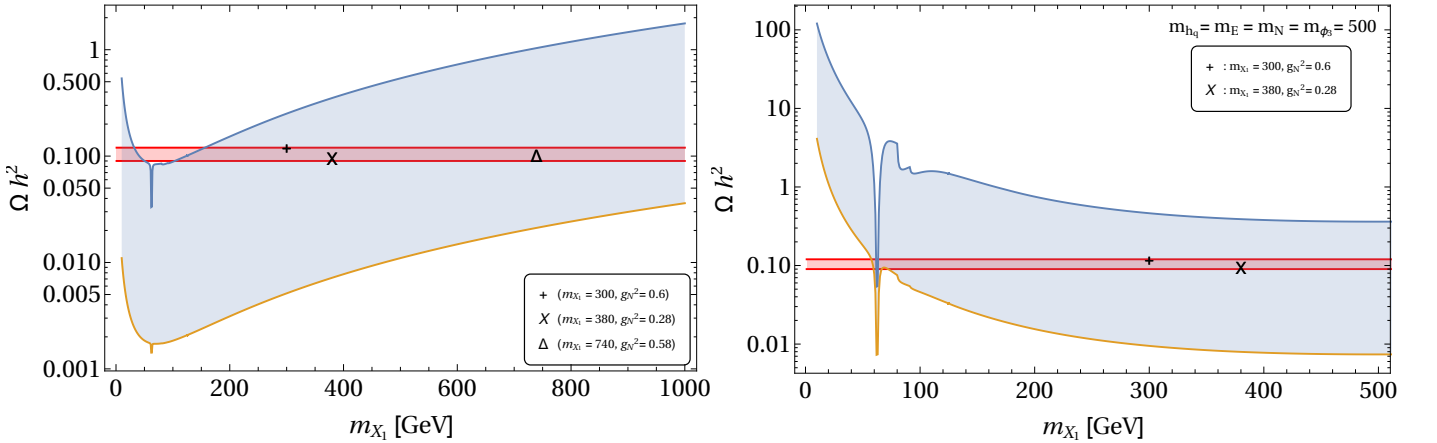


FIG. 7. The variations of relic density has been shown as a function of DM mass for two hypothesis: mass of the exotic fermions (left-panel) are proposed to be $(m_{X_1} + 100)$ GeV; and (right-panel) are fixed at 500 GeV. The $SU(2)_N$ coupling g_N^2 is also varied within the range of $\{0.32 : 0.78\}$ for each values of m_{X_1} . Correct relic density window is shown by red band. Freeze-out points of Fig. 6 are also indicated.

The patterns of the relic density contributions are different in both the plots. In the left panel the exotic fermions are always 100 GeV heavier than the dark matter mass m_{X_1} , thus when the dark matter mass increases the propagators become heavier which causes depletion in cross-section and thus the relic density increases monotonically. In the right panel, the DM is lighter than the exotic fermions, but the propagator masses are fixed at 500 GeV. Thus when m_{X_1} increases and approaches the exotic fermion masses, final state phase of annihilation increases causing an increase in cross-section and decrease in relic density. The $SU(2)_N$ gauge coupling g_N has been varied in these plots within range of $\{0.32 - 0.78\}$ for every mass of DM which causes the blue band in relic density. The horizontal red band depicts the allowed range of relic density following WMAP in 3σ range ²

$$0.09 \leq \Omega_{\text{DM}} h^2 \leq 0.12. \quad (18)$$

² PLANCK data dictates relic density in a similar range $\Omega_{\text{DM}} h^2 = 0.1196 \pm 0.0031$ [35], although a little more restrictive, do not alter the main outcome obtained in the paper.

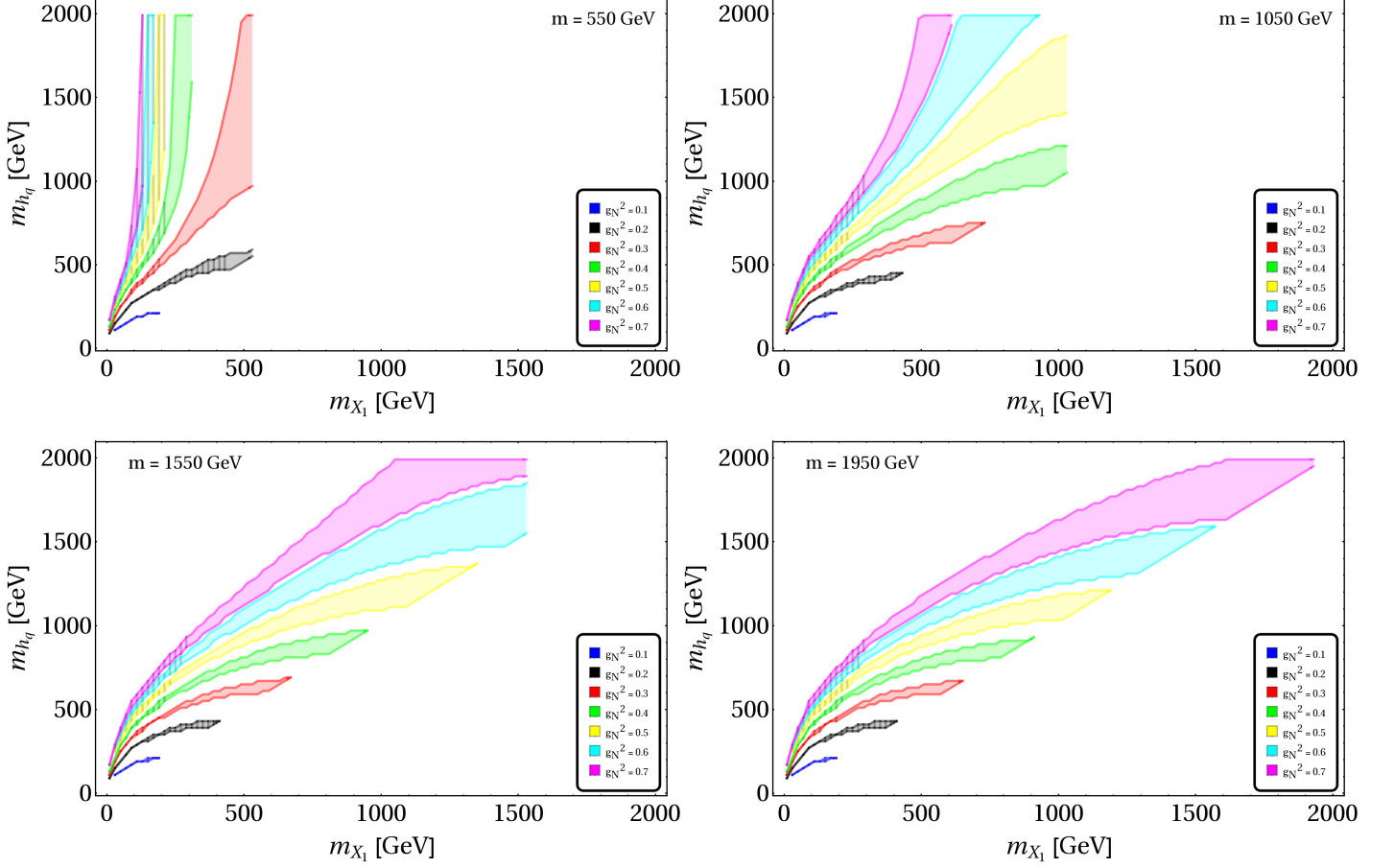


FIG. 8. Relic density allowed parameter space in $m_{X_1} - m_{h_q}$ plane for four different values of $m = m_E = m_N$: 550 GeV (top left), 1050 GeV (top right), 1550 GeV (bottom left), 1950 GeV (bottom right) for different values of $g_N^2 \rightarrow \{0.1 - 0.7\}$. The hatched region is excluded by the VEV constraints.

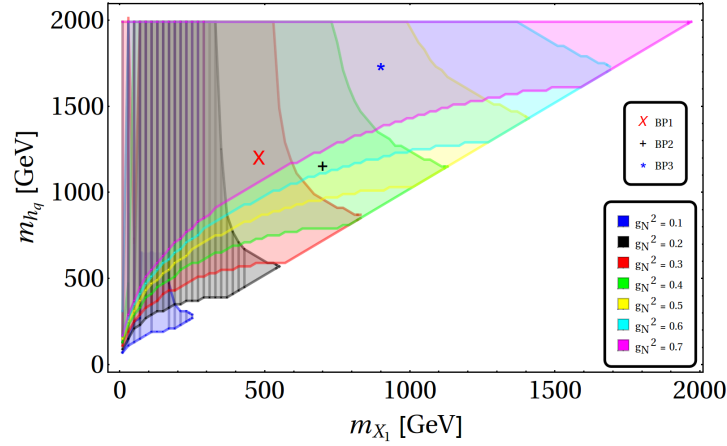


FIG. 9. Relic density allowed parameter space in m_{X_1} - m_{h_q} plane when $m = m_N = m_E$ is varied between $\{20 - 2000\}$ GeV for different $g_N^2 \rightarrow \{0.1 - 0.7\}$. The hatched region is discarded by VEV limit. Benchmark points (BP1, BP2, BP3) as discussed in Table I of the next section are also indicated in the plot.

Points that have been used to describe the freeze out of the DM in Fig. 6, (particularly both of them in the left

panel of Fig. 6 and the one with $\{m_{X_1}, g_N^2\} = \{300 \text{ GeV}, 0.6\}$ from the right panel) are indicated in Fig. 7 by (\times) , $(+)$ and (\triangle) , which fall into the red band to satisfy relic density.

Next, we would like to find the allowed region of parameter space of the model which satisfies Eq. 18. For this, we will essentially use the following variables:

$$\{g_N, m_{h_q}, m_N = m_E = m, m_{X_1}\}, \quad (19)$$

where exotic lepton and neutrino masses are merged into one single parameter m , leaving m_{h_q} out due to its dominant contribution to relic density as has already been established in Fig. 5. In Fig. 8, we have noted the allowed parameter space in $m_{X_1} - m_{h_q}$ plane for the following choices of dark gauge coupling: $g_N^2 = 0.1$ (blue), 0.2 (black), 0.3 (red), 0.4 (green), 0.5 (yellow), 0.6 (cyan), 0.7 (magenta) for four different sets of m : 550 GeV (top left), 1050 GeV (top right), 1550 GeV (bottom left), 1950 GeV (bottom right) with masses increasing gradually. It is evident that for each value of g_N (every coloured region in the plot), upper and lower boundaries correspond to maximum and minimum allowed values of m_{h_q} . This pattern is expected as we have closed the relic density criteria from both ends. For larger values of m_{h_q} , there is a depletion in annihilation cross-section causing more contribution to relic density. Thus for a given g_N to respect the maximum allowed relic density constraint, a cut-off in $m_{h_q}^{max}$ is inevitable. And once we are lowering the mass of h_q , the annihilation cross-section increases and thus the relic density decreases and hits the lower limit of allowed relic density. Thus we can summarise the plot in the following way: for every g_N , the region above and below the respective coloured region yields over and under relic density abundances. In that sense the lower region is not completely ruled out allowing for more DM components to contribute. Another important point to note here is that with larger values of m , larger values of m_{X_1} are allowed, i.e., relic density compatible annihilation cross-section can also be achieved when mass of X_1 approaches the value of m . This feature is very evident from the right-panel plot of Fig. 5. Also recall that Fig. 1 dictates that there exists a lower limit of m_{X_1} for a given value of g_N from the VEV constraints. Here, we have incorporated that VEV constraint restricting low DM mass regions, which has been shown by the hatched regions. In passing, we would like to mention that the vertical cut off in Fig. 8 indicates the maximum value allowed for m_{X_1} given a choice of m which can not be exceeded. For example, in the top left plot, m_{X_1} cannot be larger than $m = 550$ GeV. Fig. 9 shows the allowed parameter space in DM mass vs m_{h_q} plane when m is varied upto 2 TeV, which summarises the plots in all panels of Fig. 8. Three benchmark points (BP1, BP2, BP3), identified after all other constraints, are indicated in this plot and listed in Table I, .

The other important correlation between the DM mass and the coupling for satisfying right relic density is shown in Fig. 10. Here we have chosen all the exotic fermion masses to be degenerate with mass $m \geq m_{X_1}$. The blue shaded region is allowed by relic density. The grey shaded region depicts the VEV disallowance and thus excluded.

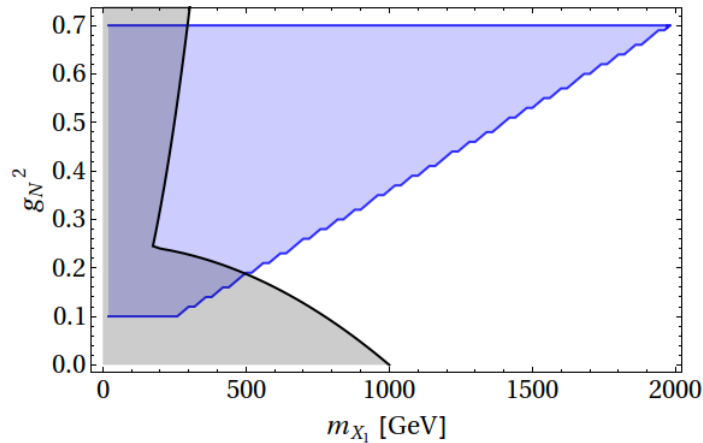


FIG. 10. Relic density compatible parameter space in $m_{X_1} - g_N^2$ plane has been described by the blue region. The grey shaded region depicts the VEV disallowance and thus excluded.

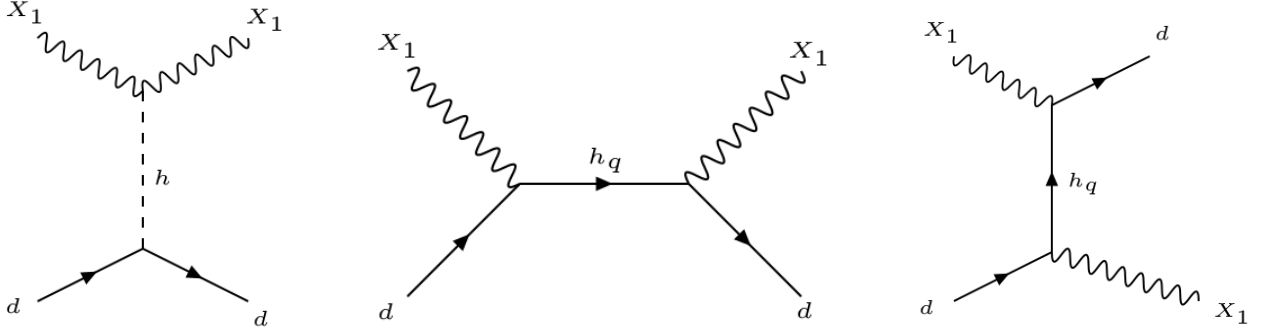


FIG. 11. The relevant interactions of dark matter (X_1) with quarks (nucleons) for direct-search experiments.

B. Direct detection constraints

The vector boson DM can scatter off the nucleus following the diagrams in Fig. 11. Spin-independent cross-section (in elastic limit) can be estimated as [43, 44]:

$$\sigma_{DD}^{SI} = \frac{1}{\pi} \left(\frac{m_{nu}}{m_{X_1} + m_{nu}} \right)^2 \left| \frac{Z f_p + (A - Z) f_n}{A} \right|^2, \quad (20)$$

where Z and $(A - Z)$ are the number of protons and neutrons respectively. The mass of nucleus is given as $m_{nu} = Am_p + (A - Z)m_n$. Here, $m_{p(n)}$ and $f_{p(n)}$ are the mass and form factor for proton (neutron).

The ratio of the form factors of proton and neutron *w. r. t.* their respective masses is computed using the diagrams in Fig. 11 and incorporating the gluonic contributions along with the twist-2 operators as :

$$\begin{aligned} \frac{f_i}{m_i} = & (I_i) \left[-\frac{g_N^2}{4m_h^2} \left(\frac{v_1}{v} \right)^2 - \frac{g_N^2}{16} \frac{m_{h_q}^2}{(m_{h_q}^2 - m_{X_1}^2)^2} \right] + \frac{3}{4} (J_i) \left[-\frac{g_N^2}{4} \frac{m_{X_1}^2}{(m_{h_q}^2 - m_{X_1}^2)^2} \right] \\ & - (K_i) \left((1.19) \frac{g_N^2}{54m_h^2} \left(\frac{v_1}{v} \right)^2 + \frac{g_N^2}{36} \left[(1.19) \frac{m_{h_q}^2}{6(m_{h_q}^2 - m_{X_1}^2)^2} + \frac{1}{3(m_{h_q}^2 - m_{X_1}^2)} \right] \right), \end{aligned} \quad (21)$$

where i stands for either proton (p) or neutron (n) and their respective form factors are $I_{p(n)} = 0.052$ (0.061); $J_{p(n)} = 0.222$ (0.330); $K_{p(n)} = 0.925$ (0.922).

Direct search cross-section limits on the vector boson DM is summarised in Fig. 12. The left-panel of Fig. 12 shows the variations of direct detection cross-section (σ_{DD}^{SI}) with DM mass m_{X_1} where mass of exotic quark m_{h_q} is being varied within relic density allowed range (recall Fig. 9) for every chosen g_N . In this plot, every g_N dependence is tagged by different colour codes, *e.g.* $g_N^2 = 0.7$ by pink, 0.1 by blue, and so on. It is worthy to note that every coloured region possesses two boundaries corresponding to maximum and minimum values of σ_{DD}^{SI} corresponding to maximum and minimum m_{h_q} involved in the scan. This is because of the s -channel contribution from h_q in Fig. 11, where h_q appears in the propagator and smaller direct detection cross section occurs with heavier m_{h_q} . The VEV disallowed points are shown by hatched regions which discard the low DM mass regions entirely, excluding small $g_N^2 = \{0.1, 0.2\}$ regions. In right-panel of Fig. 12, we have shown the variations of direct detection cross-section (σ_{DD}^{SI}) with DM mass m_{X_1} for some chosen $m_{h_q} = \{500, 800, 1100, 1400, 1700, 2000\}$ GeV where g_N^2 is varied to yield relic density allowed parameter space. Again, every coloured region corresponding to a specific m_{h_q} possesses two boundaries corresponding to maximum and minimum values of σ_{DD}^{SI} corresponding to maximum and minimum values of g_N adhered in this analysis to yield correct relic density. LUX exclusion limits are shown by the dotted black lines where the black thick line shows the sensitivity of XENON 1T experiment. The main take from this figure is to note that there exists a huge region of parameter space which lies below the LUX exclusion bound and spans almost all values of coupling and m_{h_q} masses. This is particularly because in this model, the direct search cross-section is dominated by s -channel m_{h_q} mediation unlike other DM models, where a larger propagator yields smaller direct search cross-section, and still has the freedom of utilising other exotic fermions to yield correct relic density.

Next is to revisit the relic density allowed space of the model in the light of LUX exclusion bounds. In Fig. 13, we have shown this in $m_{h_q} - m_{X_1}$ plane for different values of m_N with $g_N^2 = 0.4$. Points excluded by LUX data is shown in the left panel while those which will get discarded by XENON 1T is shown in the right panel through the

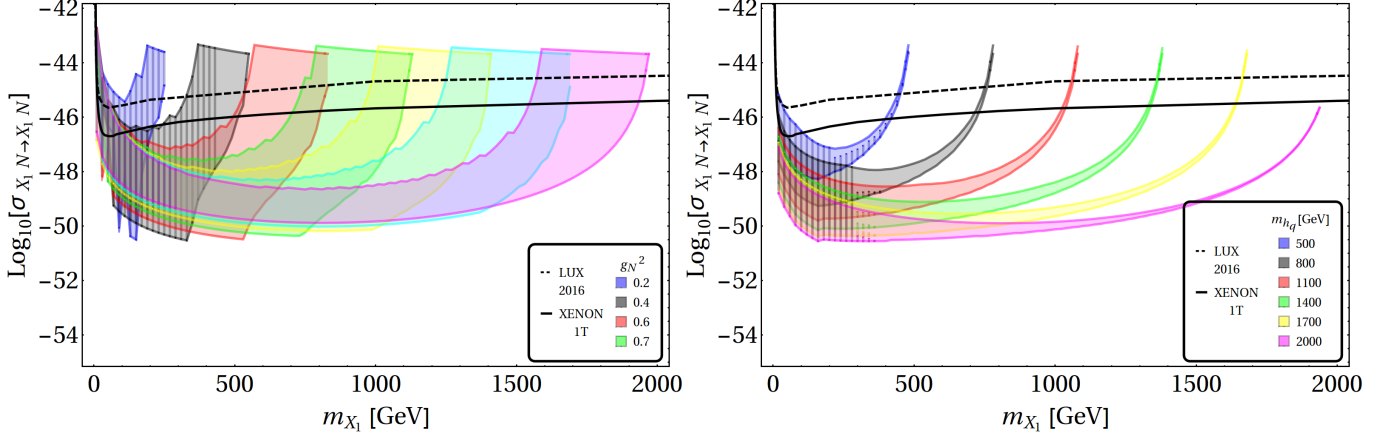


FIG. 12. Spin independent direct search cross-section for the vector boson DM X_1 with respect to DM mass (m_{X_1}) for relic density allowed parameter space. Left-panel: Different values of g_N^2 is shown by different colours where m_{h_q} is varied appropriately to yield correct relic density. Right panel: Different m_{h_q} values are shown by different coloured regions where g_N^2 is varied to yield correct relic density. LUX exclusion limit and XENON 1T prediction limits are depicted by the dashed and solid black lines respectively. VEV constraints are shown by hatched regions.

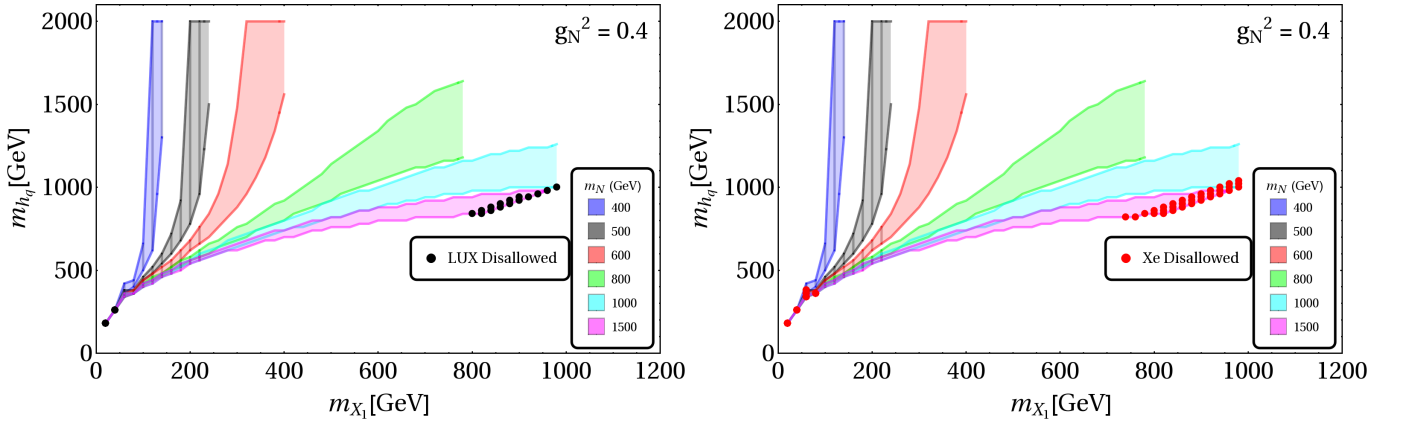


FIG. 13. Direct search exclusion limits on relic density allowed parameter space of $m_{X_1} - m_{h_q}$ plane from LUX on the left hand side and from XENON 1T on the right hand side. $g_N^2=0.4$ is chosen for illustration. Different allowed values of m_N from relic density constraint are shown in different colours. VEV constraints are shown by hatched regions.

dotted points. It shows that even for a specific coupling, the discarded region is very tiny, leaving a large region of the parameter space allowed for the model. Again, this is attributed to the presence of the s -channel direct search diagram through m_{h_q} , which yields large cross-section only in the vicinity of $m_{X_1} \sim m_{h_q}$ due to resonance. Otherwise, the heavy mass limits considered here yield very small direct search cross-section which are mostly allowed by the present bound providing the model with a golden opportunity to be probed in future XENON 1T or beyond.

C. Co-annihilation of X_1 with X_2

There are two R-charge odd gauge bosons $X_{1,2}$. In our scenario, as discussed earlier and with $m_{X_2} > m_{X_1}$, the lightest one (X_1) is stable and serves as DM candidate. However, the heavier one can contribute to the relic density of X_1 by co-annihilation to a pair of SM particles. The possible co-annihilation channels are already depicted in Figs. 2,

3, 4 where $i = 1, j = 2$. This effective total cross-section including co annihilation can be written as

$$\langle \sigma v \rangle_{eff} = (\sigma v)_{X_1 X_1 \rightarrow SM SM} + (\sigma v)_{X_1 X_2 \rightarrow SM SM} \left(1 + \frac{m_{X_1}}{m_{X_2}} \right)^{\frac{3}{2}} \exp(1 - m_{X_2}/m_{X_1}). \quad (22)$$

Similar to annihilation, co-annihilation contributions are also computed at the threshold $s_0 = (m_{X_1} + m_{X_2})^2$, yielding s - wave contributions. Co-annihilations, which can yield significant contribution only in the vicinity of $m_{X_1} \sim m_{X_2}$, otherwise has a Boltzmann suppression as shown in the last term of Eq. 22. This effectively helps the DM model to live in even a larger region of parameter space as the co-annihilation contributions do not affect the direct search of the DM. A scan of the relic density allowed parameter space of the model after incorporating co-annihilation effects is shown in the direct search cross-section versus DM mass plane in Fig. 14. Here we have chosen a specific $g_N^2 = 0.4$ for illustration. The choices of different values of m_{X_2} is varied from 600 to 1800 GeV and shown by different colour codes in Fig. 14. m_{h_q} and m_N are, varied accordingly, to satisfy relic density constraint after co-annihilation is taken into account. As we can see from the plot, that relic density allowed parameter space not only lies beyond the LUX exclusion limit, but also beyond the XENON 1T reach. The larger is the value of m_{X_2} , the larger is the DM mass for co-annihilation to contribute and the smaller is the direct search cross-section. VEV exclusion limit is shown in the left hand side by the grey band, which anyway puts a limit on the low DM mass ~ 200 GeV.

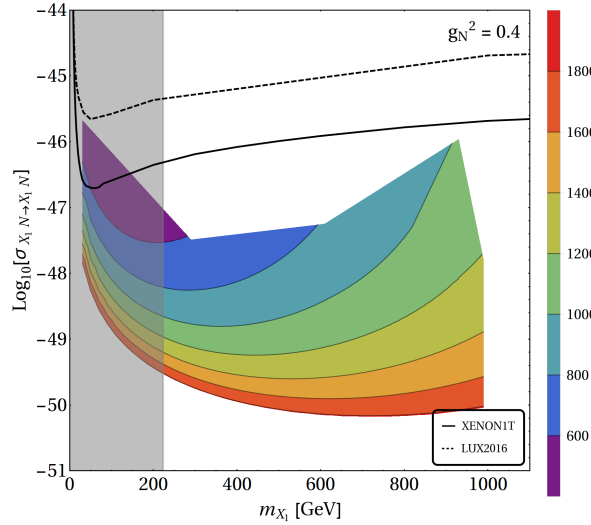


FIG. 14. Direct search cross-section for relic density allowed parameter space for X_1 with co-annihilation taken into account. m_{X_2} is varied and shown by different colour codes. LUX 2016 exclusion limits and XENON 1T sensitivity are depicted by the dashed and solid black lines respectively. VEV exclusion limit is represented by the grey region.

IV. UNIFIED FRAMEWORK UNDER $E(6)$

In this section we have queried whether the gauge symmetry of our interest, $SU(2)_L \otimes SU(2)_N \otimes U(1)_Y \otimes SU(3)_C$, can be realized within a unified scenario. To understand this we have adopted $E(6)$ as our unified group and considered the following breaking patterns to achieve the low scale theory:

$$E(6) \xrightarrow{M_U} SU(3)_L \otimes SU(3)_R \otimes SU(3)_C \xrightarrow{M'_I} SU(2)_L \otimes U(1)_L \otimes SU(2)_R \otimes U(1)_R \otimes SU(3)_c \\ \xrightarrow{M_I} SU(2)_L \otimes U(1)_Y \otimes SU(2)_N \otimes SU(3)_c \xrightarrow{M_I^N} SU(2)_L \otimes U(1)_Y \otimes SU(3)_c \xrightarrow{EWSB} SU(3)_c \otimes U(1)_{EM}$$

Below we have discussed the symmetry breaking at different intermediate scales and also using the extended survival hypothesis (ESH) we have encapsulated the beta-function coefficients [45] for gauge coupling evolutions appear for those respective scales

- $E(6)$ can be spontaneously broken to $SU(3)_L \otimes SU(3)_R \otimes SU(3)_C \equiv \mathcal{G}_{333}$ through the vacuum expectation value (VEV) of $650_H(650'_H)$ scalar keeping D-parity intact(broken). The scalar fermion fields that contribute to the

running of the couplings g_{3L}, g_{3R}, g_{3C} , gauge couplings associated with $SU(3)_L, SU(3)_R, SU(3)_C$ respectively, are³:

$$27_F = [\bar{3}, 3, 1] + [3, 1, 3] + [1, \bar{3}, 3], \quad 650'_H \supset [8, 8, 1] + [1, 8, 1], \\ 27_H \supset [\bar{3}, 3, 1].$$

Here, we would like mention that when this breaking occurs via VEV of 650_H then only $[8, 8, 1]$ will contribute in the beta-functions, and D-parity will remain conserved. This can be understood intuitively as one can see that the fields that contribute to the beta-coefficients in the running of g_{3L} and g_{3R} are identical. Thus $g_{3L} = g_{3R}$ will be maintained as long as \mathcal{G}_{333} is unbroken. We compute the beta-coefficients as:

$$b_{3L} = 7/2, \quad b_{3R} = 9/2(7/2), \quad b_{3c} = -5,$$

where the value in parenthesis denotes the respective value for the D-even case.

- $SU(3)_L \otimes SU(3)_R \otimes SU(3)_C$ is further broken to $SU(2)_L \otimes U(1)_L \otimes SU(2)_R \otimes U(1)_R \otimes SU(3)_C (\equiv \mathcal{G}_{21213})$ through VEV of $(\bar{3}, 3, 1)$. The particles that contribute in the beta-functions are read as

$$27_F = [2, -1/2\sqrt{3}, 1, -1/\sqrt{3}, 1] + [2, 1/2\sqrt{3}, 1, 0, 3] + [1, 1/\sqrt{3}, 2, 1/2\sqrt{3}, 1] + [1, 0, 2, -1/2\sqrt{3}, \bar{3}] \\ + [2, -1/2\sqrt{3}, 2, 1/\sqrt{3}, 1] + [1, 0, 1, 1/\sqrt{3}, \bar{3}] + [1, -1/\sqrt{3}, 1, 0, 3] + [1, 1/\sqrt{3}, 1, -1/\sqrt{3}, 1] \\ 27_H \supset [2, -1/2\sqrt{3}, 1, -1/\sqrt{3}, 1] + [1, 1/\sqrt{3}, 2, 1/2\sqrt{3}, 1] + [2, -1/2\sqrt{3}, 2, 1/2\sqrt{3}, 1] \\ 650_H \supset [1, 0, 3, 0, 1].$$

under the symmetry group \mathcal{G}_{21213} . The beta-coefficients are:

$$b_{2L} = -5/6, \quad b_{2R} = -5/6(1/6), \quad b_{LL} = b_{RR} = 115/18, \quad \tilde{b}_{RL} = \tilde{b}_{LR} = 1/9, \quad b_{3c} = -5.$$

- Here, \mathcal{G}_{21213} is broken to $SM \otimes SU(2)_N$ in such a way that the hypercharge generator is originated as one of the linear combination of $U(1)_L$ and $U(1)_R$ generators.

The fermion and scalar fields that contribute to the evolutions of the gauge couplings, $g_{2L}, g_{2N}, g_1, g_{3C}$, are read as

$$27_F = [2, 1, 1/6, 3] + [1, 1, -2/3, \bar{3}] + [1, 2, 1/3, \bar{3}] + [1, 1, -1/3, 3] + [2, 2, -1/2, 1] \\ + [2, 1, 1/2, 1] + [1, 1, 1, 1] + [1, 2, 0, 1] \\ 27_H \supset [2, 2, -1/2, 1] + [2, 1, 1/2, 1] + [1, 2, 0, 1] \\ 650'_H \supset [1, 3, 0, 1].$$

under the symmetry group $SU(2)_L \otimes SU(2)_N \otimes U(1)_Y \otimes SU(3)_C$ with beta-coefficients

$$b_{2L} = -5/6, \quad b_{2R} = 1/6, \quad b_{1Y} = 21/2, \quad b_{3c} = -5,$$

respectively.

The sub-multiplet $650'_H \supset [1, 8, 1] \supset [1, 3, 0, 1]$ is considered for D-parity breaking case only. This $SU(2)_N$ triplet $\Delta \equiv [1, 3, 0, 1]$ plays a crucial role in this analysis. The VEV of this triplet breaks the mass degeneracy of the $SU(2)_N$ gauge bosons, and lead to one component dark matter scenario. Otherwise for D-parity conserving case where this triplet is absent this framework will have two dark matter candidates.

- in the next step $[1, 2, 0, 1] \in 27_H$ acquires VEV which is singlet under $SU(2)_L \otimes U(1)_Y \otimes SU(3)_c$ causes spontaneous braking of $SU(2)_N$ only leading to SM gauge symmetry. The fermion and scalar fields which participate in the evolutions of gauge couplings are (read as $[SU(2)_L, U(1)_Y, SU(3)_c]$)

$$27_H \supset [2, -1/2, 1] + [2, 1/2, 1] \\ 27_F \supset [2, 1/6, 3] + [1, -2/3, \bar{3}] + [1, 1/3, \bar{3}] + [2, -1/2, 1] + [1, 1, 1],$$

³ We have relied on extended survival hypothesis (ESH) which tells that only those scalars are light which are participating in the symmetry breaking.

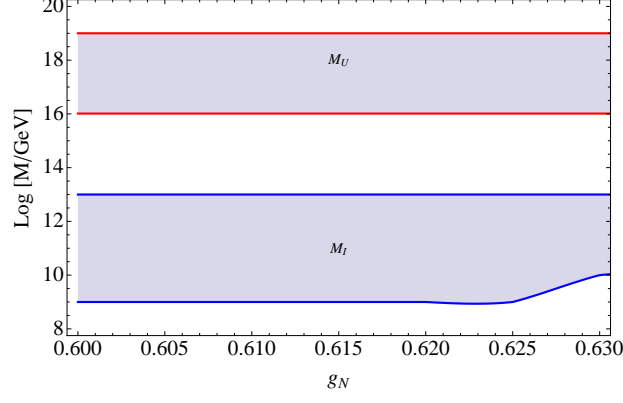


FIG. 15. The unification within D-parity odd scenario has been encapsulated. The range of $SU(2)_N$ gauge coupling, g_N , and one of the intermediate scales (M_I) have been explored with allowed unification scale (M_U), i.e., within $\{10^{18} - 10^{19}\}$ GeV. Here, M_I' is considered to be degenerate with M_U , and M_I^N is chosen to be TeV scale.

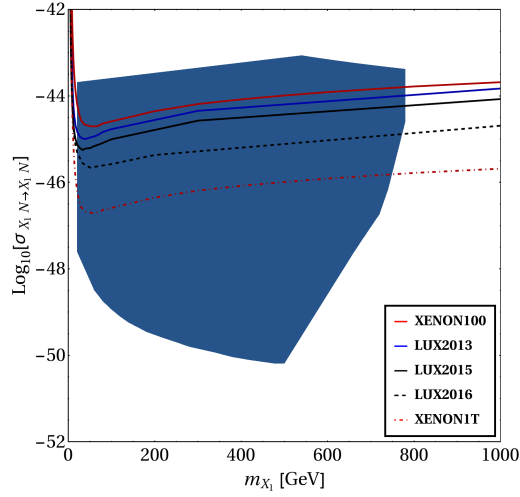


FIG. 16. Relic density allowed parameter space for degenerate DM scenario ($m_{X_1} = m_{X_2}$) in spin independent direct search cross-section vs. DM mass plane.

and the corresponding beta-coefficients are:

$$b_{2L} = -3, b_{1Y} = 21/5, b_{3c} = -7$$

associated with g_{2L}, g_{1Y}, g_{3C} respectively⁴.

Here, we have considered both D-parity conserving and non-conserving cases. The only difference is for D-parity broken case we will have one extra $SU(2)_N$ triplet at the TeV scale, and its respective parent multiplet will be there at high scales. We have introduced three intermediate symmetry groups in between $E(6)$ and the SM. In principle these intermediate scales can be different. But we have noted as almost all the fermions (27-dimensional) stick till $SU(2)_N$ breaking scale, beta coefficients for $U(1)_L$ and $U(1)_R$ are quite large ($\sim 115/18$) which causes the rapid growth of the respective gauge couplings and make them non-perturbative immediately. Thus to avoid such catastrophe we have assumed that \mathcal{G}_{333} is broken directly to $SM \otimes SU(2)_N$ directly, i.e. M_I coincides with M_I' . Thus in our scenario

⁴ Here, g_1 is the GUT normalized $U(1)_Y$ coupling, and we have used the normalization factor $3/5$ to fit it within this framework.

M_I^N and M_I are free parameters. The choice of M_I^N is constrained from the phenomenological considerations in this analysis and which is around TeV. We have also restricted our unification scale to be within $[10^{19} : 10^{16}]$ GeV. For D-parity broken scenario we find ranges of g_N and M_I compatible with unification respecting the proton decay constraint. We have noted the allowed range of g_N is $[0.60 : 0.63]$, see Fig. 15.

For D-parity even case, g_N is no more free parameter and equals to g_{2L} . Here, also we find consistent solutions for unification with M_I ranges between $[10^{19} : 10^{16}]$ GeV. This D-parity even case will lead to degenerate mass for the dark matter $X_{1,2}$ as the triplet VEV is absent here. Thus we will have a degenerate two component dark matter scenario which is itself an interesting possibility but turns out to be not viable by the relic density and direct search constraints as shown in Fig. 16. It shows that for the degenerate DM scenario with $m_{X_1} = m_{X_2}$, relic density allowed region is only possible within $m_{X_1} < 1$ TeV which goes against the condition of $m_{X_1} = m_{X_2} = m_{X_3} = 1$ TeV which can't be avoided. Hence, D-parity even case with degenerate DM doesn't work for this model and we have to focus only on the D-parity broken scenario with a single component DM.

A. Summary of dark matter phenomenology

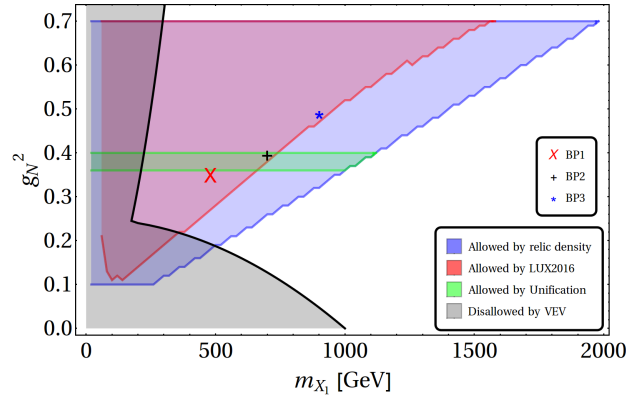


FIG. 17. Relic density (blue shaded), direct search (red shaded) and unification (green shaded) allowed parameter space in $g_N^2 - m_{X_1}$ plane. Three chosen benchmark points BP1, BP2 and BP3 (see Tab. I) are also shown.

Benchmark Points	g_N	m_{X_1} (GeV)	m_{X_2} (GeV)	m_{h_q} (GeV)	m (GeV)	Ωh^2	σ_{DD} (cm ²)
BP1	0.59	480	1000	1200	600	0.09	10^{-50}
BP2	0.63	700	1000	1160	860	0.1	10^{-49}
BP3	0.70	900	1000	1740	920	0.09	10^{-49}

TABLE I. Three benchmark points (BP1, BP2, BP3) of the model are identified with input parameters $\{g_N, m_{X_1}, m_{h_q}, m = m_N = m_E\}$. Relic density and direct detection cross-sections for these points are also mentioned. We have set m_{X_2} at 1000 GeV to obey maximum splitting scenario (see Eq. 3).

Before we proceed further, we would like to summarise the outcome of DM phenomenology in the light of relic density, direct search and unification constraints. In Fig. 15, we have adjudged the correlation amongst two parameters which crucially govern DM phenomenology of dark $SU(2)_N$ gauge sector, namely DM mass and the coupling. As we have argued to stick to D-parity broken scenario, g_N is not identical to $SU(2)_L$ coupling and in principle is a free parameter and hence DM mass (m_{X_1}) is a function of g_N and $SU(2)_N$ symmetry breaking VEVs ($\kappa_2, \delta_{1,2}$). In Fig. 10, on top of relic density allowed (blue shaded) and VEV disallowed (grey shaded) parameter space in $\{m_{X_1}, g_N\}$

plane, we incorporated direct detection constraint provided by LUX 2016 data in red shaded region and unification constraint by green shaded region. Essentially direct search kills the edge of the relic density allowed parameter space where approximately $m_{X_1} \sim m_{h_q}$ as has already been noted. The green horizontal strip depicts the allowed range of g_N on the other hand has already been derived which shows the breathing space beyond SM $SU(2)_L$ coupling to satisfy unification for D -parity broken scenario. For further phenomenological exploration in context of the Large Hadron Collider (LHC), we have chosen three benchmark points (BPs) which are pointed out in Fig. 15 by BP1 (\times), BP2 (+), BP3 (\star). These benchmark points with the input parameters, relic density and direct search cross-sections are detailed in Tab. I. We have chosen the BPs with varying DM mass from 500 GeV to \sim TeV. As we have been pointing out to the maximum splitting scenario (see Eq. 3) where $m_{X_2} \sim m_{X_3}$, we have chosen $m_{X_2} = 1$ TeV to obey the observed limit on a heavy neutral gauge boson mass. We also have chosen different g_N for these benchmark points, two of which (BP1 and BP2) falls within the unification window. For BP3 a larger coupling is chosen, which is adjusted by a large DM mass to yield relic density and direct search in the right ball park. Even after specifying DM mass and coupling, choice of m_{h_q} and m_N has some freedom to yield correct relic density and direct search bound, but the values chosen here have been motivated from a specific hierarchy of $m_{h_q} > m_{X_2} > m_N > m_{X_1}$ as we will shortly discuss in collider phenomenology. Also note that, excepting for the last point BP3, others have negligible co-annihilation contributions due to large mass difference between m_{X_1} and m_{X_2} .

V. COLLIDER PHENOMENOLOGY AT LHC

Collider signatures of this model is an interesting phenomena with large number of particles introduced. There are exotic fermions including heavy quark (h_q), heavy lepton (E) and heavy neutrino (N), heavy scalars and three neutral additional gauge bosons one of which serves as DM (X_1) yielding a lot of possibility of studying collider signatures of this model. In this draft, we will only highlight two possibilities that yield multi-leptonic final states at the LHC, namely:

- Opposite sign dilepton plus a single jet and missing energy (OSD: $\ell^+\ell^- + 1\ j + \cancel{E}_T$),
- Hadronically quiet four lepton and missing energy (HQ4l: $2\ell^+2\ell^- + \cancel{E}_T$).

Leptonic final states are interesting for study at LHC as the background contribution from SM is relatively less. Unfortunately no excess has been reported from the existing data yet. Hence, we will provide a rough estimate of the limit of the excitation involved in the production from the existing data and predict future prospect of the model at the higher centre-of-mass energy and luminosity runs of LHC. Our discussion will be based on the final state event selection and accordingly we will discuss signal and background contributions in each of the cases. Before, we will discuss the simulation criteria.

A. Simulation methodology

We have implemented our model in CalcHEP [46] and generated parton level events. The parton level events have been fed into PYTHIA v.6 [47] for showering and hadronization. Here, we have performed the analysis with center of mass energy $\sqrt{s} = 14$ TeV. We have used CTEQ6L [48] parton distribution function with renormalisation (μ_R) and factorisation (μ_F) scales set to the sub-process center mass energy.

All the exotic particles eventually decay into leptons and jets with DM providing missing energy which consists our variety of event selections as described above. However, to mimic the experimental environment we use the following suggested identification criteria:

- *Lepton* ($\ell = e, \mu$): They are identified with minimum transverse momentum (p_T) of 20 GeV, and with pseudo-rapidity $|\eta| < 2.5$ to identify them in the central region of the detector. Two leptons are treated as isolated objects if their mutual separation satisfy $\Delta R = \sqrt{(\Delta\eta)^2 + (\Delta\phi)^2} \geq 0.2$. Lepton-jet separation must satisfy $\Delta R \geq 0.4$. τ leptons are difficult to observe in electromagnetic and muon calorimeter due to their decay and so they are not usually classified into lepton category.
- *Jet* (*jet*): Partons after emerging out of the collision vertex form hadrons due to $SU(3)$ interactions which cluster to form jets. We have used the PYCELL jet formation algorithm inbuilt within PYTHIA to define the clustered hadrons as *jets*. The detector is assumed to span $|\eta| \leq 5$ and segmented in 100- η and 70- ϕ bins. The minimum transverse energy E_T of each cell is taken as 0.5 GeV, while we require $E_T \geq 2$ GeV for a cell to act as a jet initiator. All the partons within $\Delta R = 0.4$ from the jet initiator cell are included in the formation of

the jet, and we require $E_T \geq 20$ GeV for a group to be considered a jet. We also impose a cut for the isolation of the jets from those unclustered objects (see below) to have a minim separation $\Delta R > 0.4$.

- *Unclustered Objects*: All the other final state particles, which are not isolated leptons and separated from jets by $\Delta R \geq 0.4$ are considered as unclustered objects. This clearly means all the particles (electron/photon/muon) with $0.5 < E_T < 10$ GeV and $|\eta| < 5$ and jets with $0.5 < E_T < 20$ GeV and $|\eta| < 5$, which leave their presence in the detector, are considered as unclustered objects.
- *Missing energy ($E_{\cancel{T}}$)* : DM produced in the decay chain of the exotic particles will be missed in the detector. However, the momentum imbalance in the observable particles like leptons and jets produced will indicate the transverse momentum carried by the invisible particles produced and is called missing energy which can be defined as

$$E_{\cancel{T}} = (p_T)_{mis} = -(p_T)_{vis}, \quad (p_T)_{vis} = \sqrt{(\sum_{\ell,j} p_x)^2 + (\sum_{\ell,j} p_y)^2}. \quad (23)$$

Please note that the negative sign do not carry any significance here and we will always refer to the mod value of the visible momentum as missing energy. We also note here that missing energy identification takes into account of the unclustered objects as well which do not fall into the lepton and *jet* category as defined above.

We have generated SM background events using MADGRAPH [49] and showered them in PYTHIA [47]. We have appropriately used K factor to match next to leading order (NLO) of available cross-sections for the processes contributing as SM background. There are a few shortcomings of the analysis. For example, as an artefact of using CalCHEP event generator, the spin correlation in the decay chain is not maintained; smearing effects of leptons, jets and unclustered objects are ignored; jet formation criteria is best done with anti- K_T algorithm which is not possible within PYCELL etc. In spite of all these, the discrepancy if any, is assumed to be less than 10% as we are not after any pathological corner of the detector or addressing any exotic region of the model parameter space. In that sense, even more important would have been to consider NLO effects of the signal cross-section which involves color particles in the production level which as a result can get significant corrections.

B. Opposite sign dilepton signal

Opposite sign dilepton signature arises in the model mainly due to $pp \rightarrow h_q X_1$ production through the Feynman graphs shown in the top panel of Fig. 18. The variation in production cross-section of $\sigma(pp \rightarrow h_q X_1)$ at LHC with centre-of-mass-energy of 14 TeV is shown in the bottom panel of Fig. 18 with respect to m_{h_q} keeping the DM mass m_{X_1} fixed at 480 GeV (as in BP1).

Now h_q can only decay via $h_q \rightarrow dX_{1,2}$ as shown in Fig. 19. The decay branching fraction to either of them is subject to $X_{1,2}$ masses as has been shown in Fig. 20 in terms of DM mass. With a fixed m_{X_2} and m_{h_q} , the branching fraction to dX_2 increases with larger and larger DM mass. With $h_q \rightarrow dX_1$, the production of $pp \rightarrow h_q X_1$ will end in a jet plus missing energy signature which is a standard signature which many DM models including those of minimal scalar singlet extensions provide. The background for this final state is also huge and hence reducing the background is a difficult task if not impossible. However, if we choose the following hierarchy in the spectrum:

$$m_{h_q} > m_{X_2} > m = m_E = m_N > m_{X_1}. \quad (24)$$

then X_2 can decay to $X_2 \rightarrow N\bar{\nu}$, E^+e^- , see Fig. 21, where the branching fraction to neutrino and charged lepton final states are equal in the limit of exotic neutrino and electron having the same mass $m_N = m_E$ which has been the assumption throughout the analysis. Now, the exotic leptons will decay as $N \rightarrow \nu X_1$; $E \rightarrow eX_1$ as shown in Fig. 22 with 100% branching fraction as X_2 is assumed heavier than both of the exotic leptons. If we consider $X_2 \rightarrow E^+e^-$ or the charge conjugate, will lead to a opposite sign dilepton, a soft jet and missing energy in the final state as desired. A parameter space scan for all the DM allowed region where above hierarchy is maintained is a difficult task and we will do the analysis for the selected benchmark points BP1, BP2 and BP3 which characterise the available DM parameter space of the model allowing the required final states. We have identified the SM processes which can mimic our signal, and thus considered as backgrounds. Such processes are $t\bar{t} + jets$, $WW + jets$, $WZ + jets$, $ZZ + jets$, $Zt\bar{t}$, and also the *Drell – Yan*. One of the primary kinematic variables in the DM model with a sufficiently heavy DM is missing energy ($E_{\cancel{T}}$) which is characteristically different from that of that of the SM where missing energy contributions come from neutrinos only and with energy mismatch. Missing energy distribution for the signal process $pp \rightarrow h_q X_1$ following the decays to opposite sign dilepton events for the benchmark points are plotted with the dominant SM

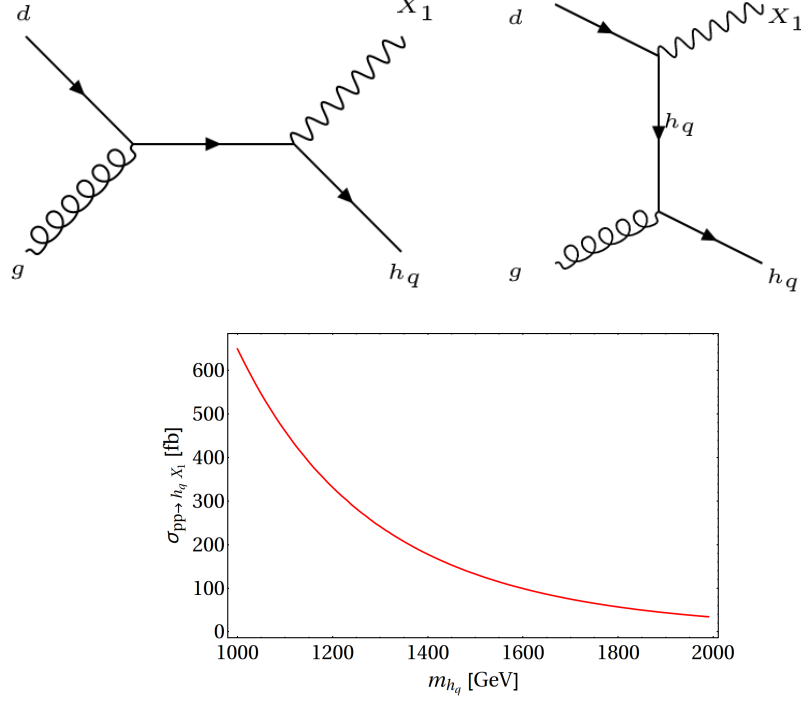


FIG. 18. Top panel: Feynman diagrams for producing h_q along with X_1 at the LHC. Bottom panel: Production cross-section at LHC for $\sqrt{s} = 14$ TeV as a function of m_{h_q} keeping the DM mass fixed at $m_{X_1} = 480$ GeV

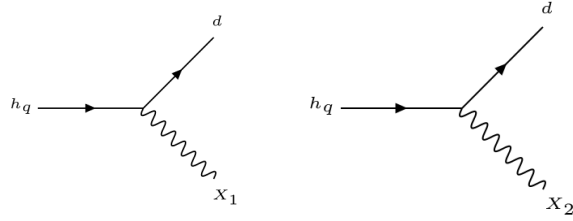


FIG. 19. Feynman diagrams of possible decay modes of h_q .

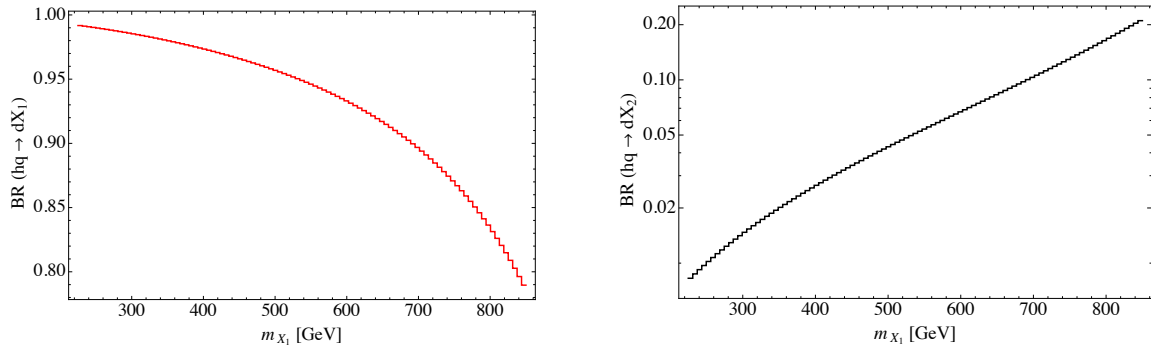


FIG. 20. Left-panel: $\text{BR}(h_q \rightarrow dX_1)$, and Right-panel: $\text{BR}(h_q \rightarrow dX_2)$ have been shown as a function of m_{X_1} where we have chosen $m_{h_q} = 1160$ GeV and $m_{X_2} = 1000$ GeV.

backgrounds in Fig. 23. As we can clearly see that missing energy for the signal picks up at a very large value while the ones for the background picks up at a very small value. This feature allows us to discriminate the model from the

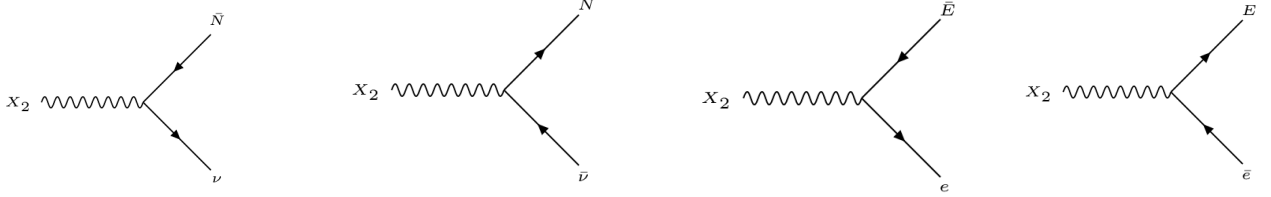


FIG. 21. Feynman diagrams showing decays of X_2 to $N \bar{\nu}$, $E^+ e^-$ and their conjugate final states.

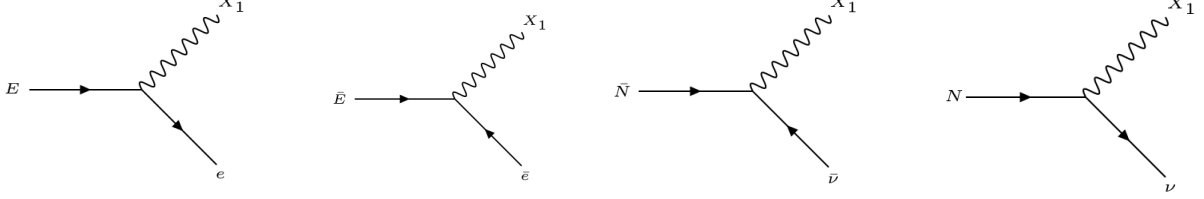


FIG. 22. Feynman diagrams showing decays of E and N to X_1 and the SM particles.

background after putting a sufficiently large missing energy cut, which retains the signal while reduces the background significantly.

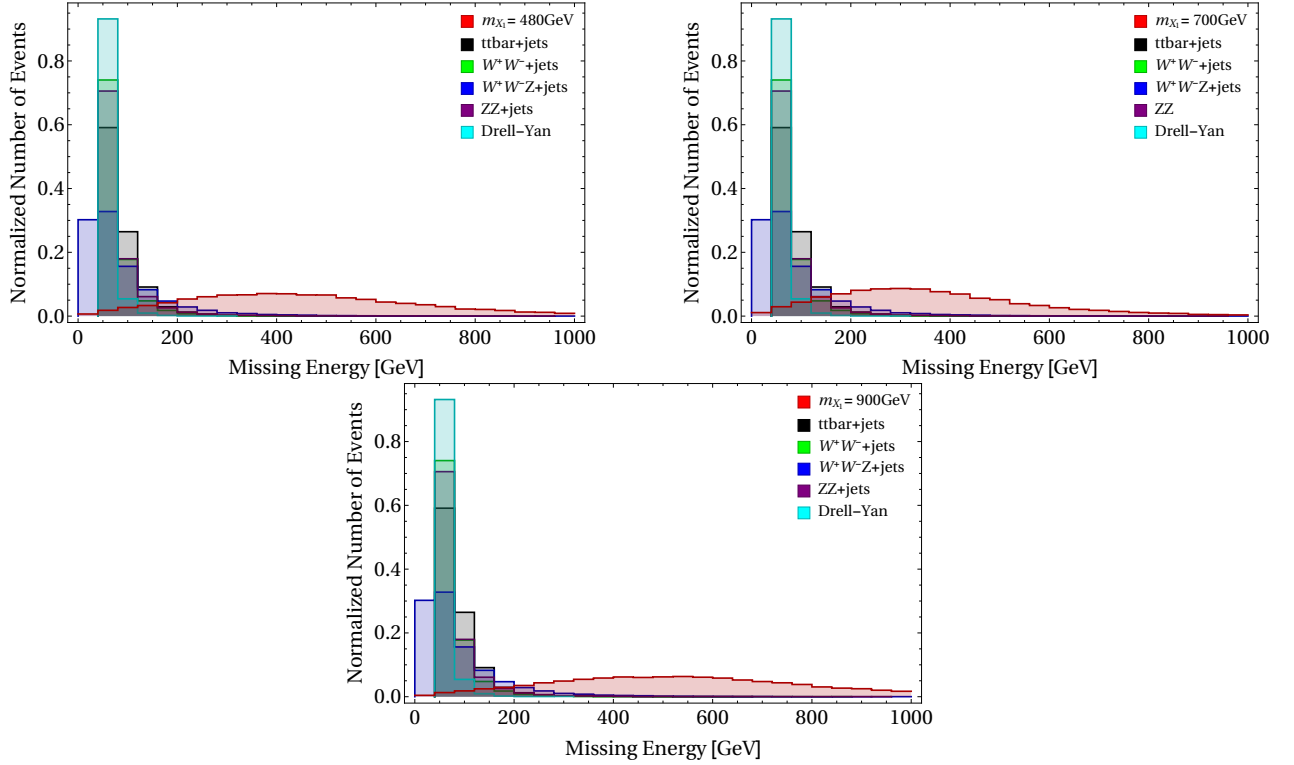


FIG. 23. Missing energy distribution for $(\ell^+ \ell^- + 1j + E_T)$ events produced at LHC from $pp \rightarrow h_q X_1$ for the benchmark points with dominant SM background. Top left: BP1, Top right: BP2, Bottom: BP3.

Another interesting feature emerges from the missing energy distribution, when we compare those only for the chosen signal benchmark points in Fig. 24 (BP1 in red, BP2 in green and BP3 in blue). Peak of the missing energy distribution depends on what momentum is being carried away by the DM. Here as m_{h_q} and DM are produced, where the $m_{h_q} > m_{X_1}$, larger part of the momentum will be carried by the exotic quark. Hence, the DM arising from h_q decay will dictate the missing energy distribution. Hence, the peaks of the distribution will depend on $\Delta m = m_{h_q} - m_{X_1}$,

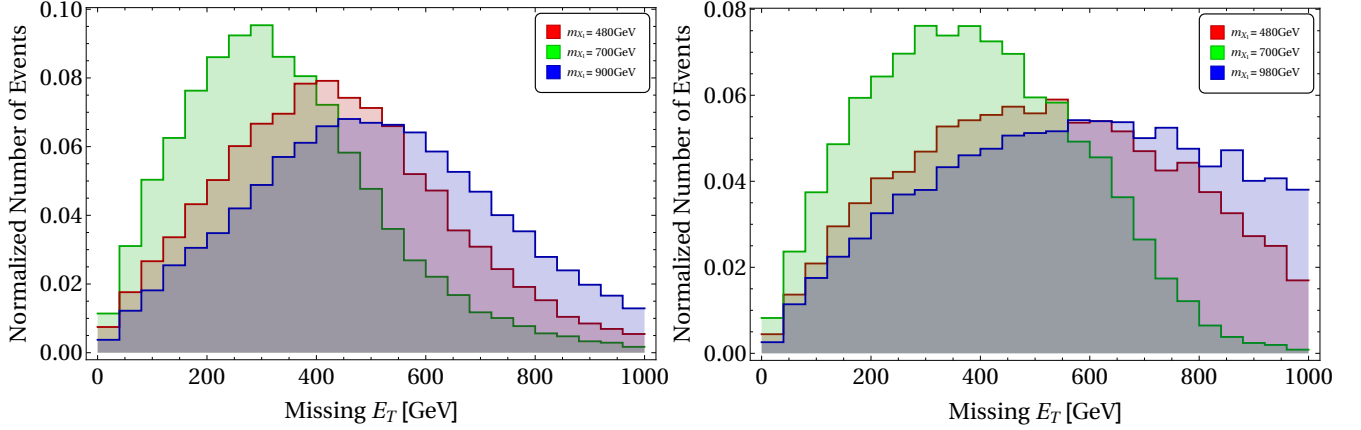


FIG. 24. Missing energy distribution for benchmark points (BP1, BP2, BP3). Left: $pp \rightarrow h_q X_1$, Right: $pp \rightarrow h_q \bar{h}_q$.

the large it is the peak will also be at a larger value. For BP1, $m_{h_q} = 1200$, $m_{X_1} = 480$, $\therefore m_{h_q} - m_{X_1} = 720$ GeV; for BP2: $m_{h_q} - m_{X_1} = 1160 - 700 = 460$ GeV and for BP3: $m_{h_q} - m_{X_1} = 1740 - 900 = 840$ GeV, yielding the peak $E_{\cancel{E}}$ for BP2 at lower value, peak for BP3 at larger value with BP1 peak in between. This in turn can help distinguishing different model points or deciphering the mass of the exotic quark, given a knowledge of DM mass from direct search experiment. We will elaborate more on this aspect in a separate draft. We have shown the missing energy distribution for two different production processes: on left: $pp \rightarrow h_q X_1$ and on the right: $pp \rightarrow h_q \bar{h}_q$.

Now, we would like to draw the attention of the reader that there is another possibility of generating same final state ($\ell^+ \ell^- + 1j + E_{\cancel{E}}$), but from a different production process $pp \rightarrow h_q \bar{h}_q$ as shown in upper panel of Fig. 25. the production cross-section is larger than the previous one ($h_q X_1$), however, the subsequent decay yields equivalent contributions as we will show in a moment. For example, if we consider one of the exotic quark decay as $h_q \rightarrow dX_1$ and the other via $h_q \rightarrow dX_2 \rightarrow de^+e^-X_1$ as in Fig. 21 22, we end up getting opposite sign dilepton but with 2 jets plus missing energy. However, one must note here that due to large momentum being carried away by $X_{1,2}$ from the decay of h_q , the jets produced are often very soft and fails to register at the detector with a threshold of $p_T = 20$ GeV in many of the events. Hence, this will contribute significantly to the opposite sign dilepton signal considered here with a single jet and missing energy.

The cross-sections in terms of actual number of events for a specific luminosity for OSD ($\ell^+ \ell^- + 1j + E_{\cancel{E}}$) events has been tabulated in Table II. On top of the basic cuts, we implemented

- Missing Energy cut: $E_{\cancel{E}} > 100, 200, 300$ GeV to reduce backgrounds.
- Invariant mass cut: $m_{\ell\ell}$ of opposite sign same flavour dilepton as has been defined in the following text is required not to lie within $m_z \pm 15$ GeV to reduce background events from Z production as we discuss later.
- For jets, a moderate $p_T > 40$ GeV is demanded. This is particularly because of the fact that the jets produced carry only a small fraction of the momentum and will be soft mostly.

We would like to note here that the number of events (N) for the desired final state mentioned in the table uses production cross-section σ_{pr} , number of events generated N_1 , number of final state events obtained N_2 (after putting all the cuts) and luminosity \mathcal{L} as

$$N = \frac{\sigma_{pr} \times N_2 \times \mathcal{L}}{N_1}. \quad (25)$$

Cross-sections of the dominant background processes contributing to OSD final state is tabulated in Table III. We have multiplied the cross-section generated at LO in **Madgraph** by appropriate K factors to match the NLO cross-section available in the literature. For example, for $t\bar{t}$: $K = 1.31$, WWj : $K = 1.30$, WZj : $K = 1.27$, ZZj : $K = 1.31$, $Drell - Yan$: $K = 1.2$ [49]. Note that these K -factors are available for $E_{cm} = 13$ TeV, but we hope it doesn't alter too much to $E_{cm} = 14$ TeV. Note that with the limitation of the number of events for which these background events are generated are often not enough to yield even one event in the desired final state with the specific cut, then we estimate a limit on the final state cross-section as follows: if a simulation with N events produces less than 1 event in a desired final state with specific cuts for a process with production cross section σ_{pr} ,

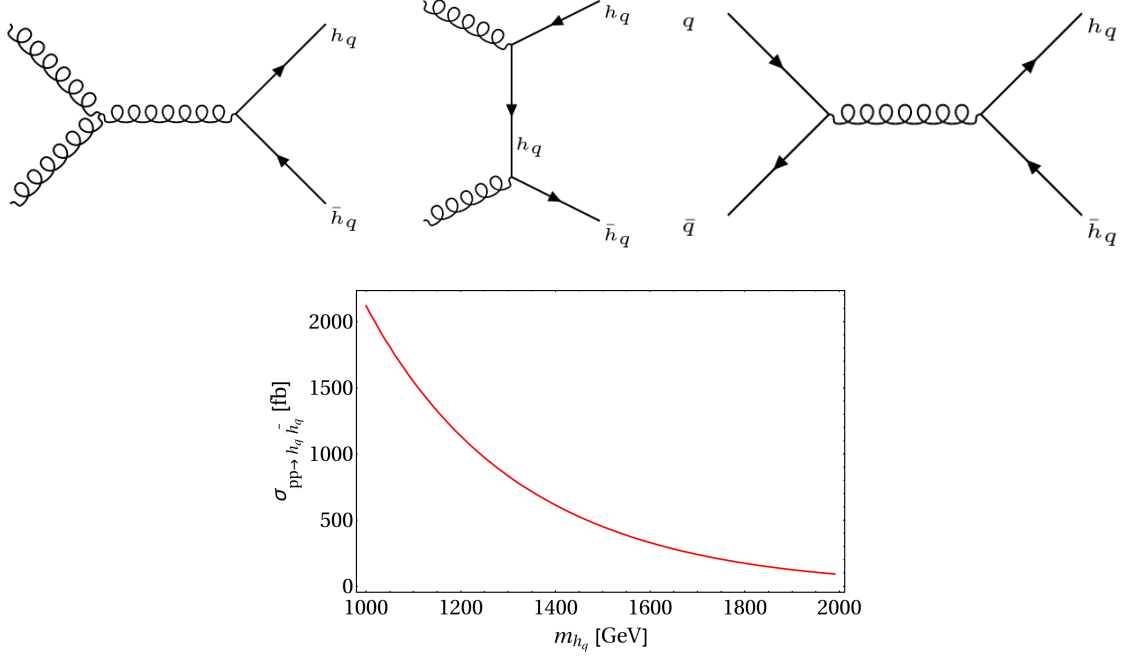


FIG. 25. Top panel: Feynman diagram for producing $h_q \bar{h}_q$ at the LHC. Bottom panel: Production cross-section ($pp \rightarrow h_q \bar{h}_q$) at LHC for $\sqrt{s} = 14$ TeV as a function of m_{h_q} .

Benchmark Points	$\sigma_{pp \rightarrow h_q X_1} (in pb)$	$\sigma_{pp \rightarrow h_q \bar{h}_q} (in pb)$	E_T^{miss}	$\sigma_{pp \rightarrow h_q X_1}^{OSD} (in pb)$	$\sigma_{pp \rightarrow h_q \bar{h}_q}^{OSD} (in pb)$	$N(100 fb^{-1})$
BP1	3.31×10^{-1}	1.13	> 100	2.94×10^{-3}	1.46×10^{-3}	440
			> 200	2.51×10^{-3}	1.24×10^{-3}	375
			> 300	1.68×10^{-3}	1.13×10^{-3}	281
BP2	1.72×10^{-1}	7.58×10^{-1}	> 100	2.35×10^{-3}	2.65×10^{-3}	500
			> 200	1.65×10^{-3}	2.04×10^{-3}	369
			> 300	9.03×10^{-4}	1.51×10^{-3}	241
BP3	1.99×10^{-2}	1.02×10^{-1}	> 100	4.87×10^{-4}	2.29×10^{-4}	70
			> 200	4.40×10^{-4}	2.24×10^{-4}	66
			> 300	3.78×10^{-4}	2.04×10^{-4}	57

TABLE II. OSD ($\ell^+ \ell^- + 1jet + \cancel{E}_T$) events for chosen benchmark points with $p_{T_\ell} > 20$, $p_{T_j} > 40$ and $|m_Z - 15| \not\leq m_{ll} \not\leq |m_Z + 15|$ at $\sqrt{s} = 14$ TeV and number of events predicted for $\mathcal{L} = 100 fb^{-1}$ luminosity.

then that final state event cross-section (σ_e) must be : $\sigma_e < \sigma_{pr}/N$. What we see from Table II and III is that BP1 and BP2 has finite probability of getting unravelled at LHC while for BP3 it is slightly harder and one requires high luminosity LHC for this. A discovery significance for oppoosite sign dilepton channel is shown in Fig. 26.

One important point in order to conclude discussion of this event. Opposite sign dilepton searches have been done exhaustively at LHC, particularly because supersymmetry provides with such a signal so very often. However, one important aspect of all those analysis is to put a very heavy effective mass $H_T = \sum_{jet} (p_T)_{jets}$ cut to segregate between signal and background. However, as we are pointing out that our model rather yields a jet with very low transverse momentum. There are essentially two different analysis that have been performed by CMS [50, 51] and ATLAS [52]: on the Z -mass window and out of the Z -mass window. In both cases CMS and ATLAS have used a strong effective mass cut and H_T on jet transverse momenta, due to which signals from vector boson DM could also be washed out. It is therefore not also quite possible to put a bound on the DM mass or on the exotic quark mass from the available LHC data. However, to be on safe side, our choices of h_q mass is sufficiently heavy (as much as the squarks in SUSY) to evade bounds from non-observation of this signal at 13 TeV data.

Process	$\sigma_{production}(in\ pb)$	E_T^{miss}	$\sigma^{OSD}(in\ pb)$	$N(100fb^{-1})$
$t\bar{t} + j$	815.50	> 100	1.32	132927
		> 200	0.057	5708
		> 300	< 0.0081	< 1
$WW + j$	60.58	> 100	0.11	11389
		> 200	0.013	1332
		> 300	3.02×10^{-3}	302
$WZ + j$	0.15	> 100	5.85×10^{-4}	58
		> 200	1.35×10^{-4}	13
		> 300	8.25×10^{-5}	8
$ZZ + j$	7.59	> 100	1.13×10^{-3}	113
		> 200	$< 3.79 \times 10^{-4}$	< 1
		> 300	$< 3.79 \times 10^{-4}$	< 1
$Drell - Yan$	703.35	> 100	0.028	2813
		> 200	$< 7.03 \times 10^{-3}$	< 1
		> 300	$< 7.03 \times 10^{-3}$	< 1

TABLE III. OSD($\ell^+\ell^- + 1jet + \cancel{E}_T$) events for dominant SM background with $p_{T_\ell} > 20$, $p_{T_j} > 40$ and $|m_Z - 15| \not\leq m_{ll} \not\leq |m_Z + 15|$ at $\sqrt{s} = 14$ TeV and $\mathcal{L} = 100\text{ fb}^{-1}$ luminosity. Appropriate K -factors are used for different processes to match to the NLO-NLL cross-sections available in literature (see text for details).

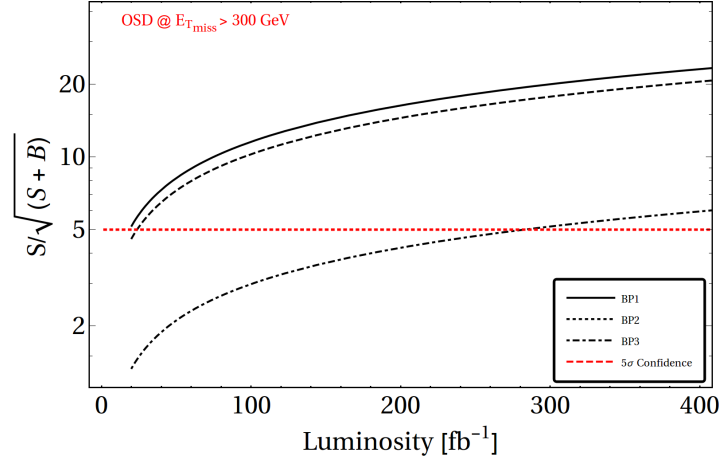


FIG. 26. Significance plot of opposite sign dilepton events with $\cancel{E}_T > 300$ GeV with luminosity.

C. Hadronically quiet four lepton signal

One of the unique channels that this model offers is hadronically quiet four lepton signature. This can easily appear from producing the heavier $SU(2)_N$ gauge boson following the Feynman graph in left panel of Fig. 27 following decays of X_2 through exotic leptons as pointed in Fig. 21 and in Fig. 22. Essentially this final state here is also an artefact of the mass hierarchy as pointed out in Eq. 24. The production cross-section is much smaller for the process as it is only a $SU(2)_N$ process and with heavier m_{X_2} , this falls off sharply to a vanishingly small value as shown in the right panel of Fig. 27. We again note here that there will be contributions to this channel from the production of $pp \rightarrow h_q \bar{h}_q$ where in both legs h_q decays via $h_q \rightarrow dX_2$ with $X_2 \rightarrow e^+e^-X_1$ through exotic charge leptons. Although the number of signal events is small in this case, the number of SM background is even more rare. ZZ , $WWWW$, $Zt\bar{t}$ only contributes dominantly. Again, we show that missing energy is one of the main discriminators for separating signal and background apart. This is shown in Fig. 28 for three benchmark points and for the dominant SM background where missing energy cut can be effectively used for separating signal from the background. The

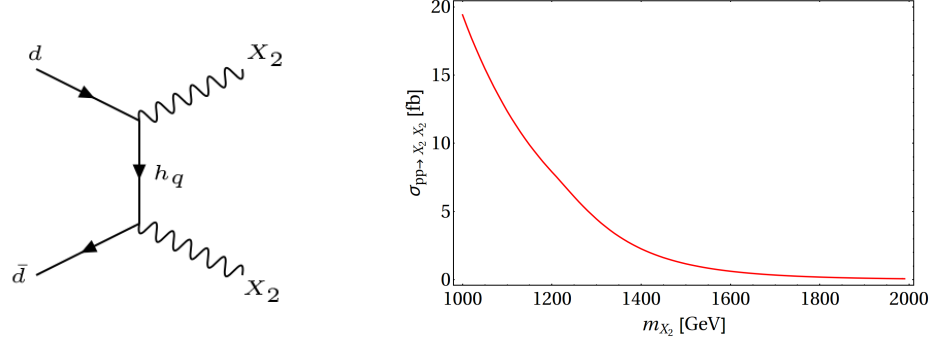


FIG. 27. Left: Feynman diagram for producing a pair of X_2 at the LHC. Right: Cross-section of $pp \rightarrow X_2 X_2$ as a function of m_{X_2} at 14 TeV LHC.

event selection criteria remains similar. We tabulate the signal and background events in IV and V respectively. For SM background, we have multiplied the cross-section generated at LO in **Madgraph** by appropriate K factors to match the NLO cross-section available in the literature. For example, for $WWWW$: $K = 1.74$, ZZ : $K = 1.29$, $Zt\bar{t}$: $K = 1.44$ [49]. Note that these K -factors are available for $E_{cm} = 13$ TeV, but we hope it doesn't alter too much to $E_{cm} = 14$ TeV.

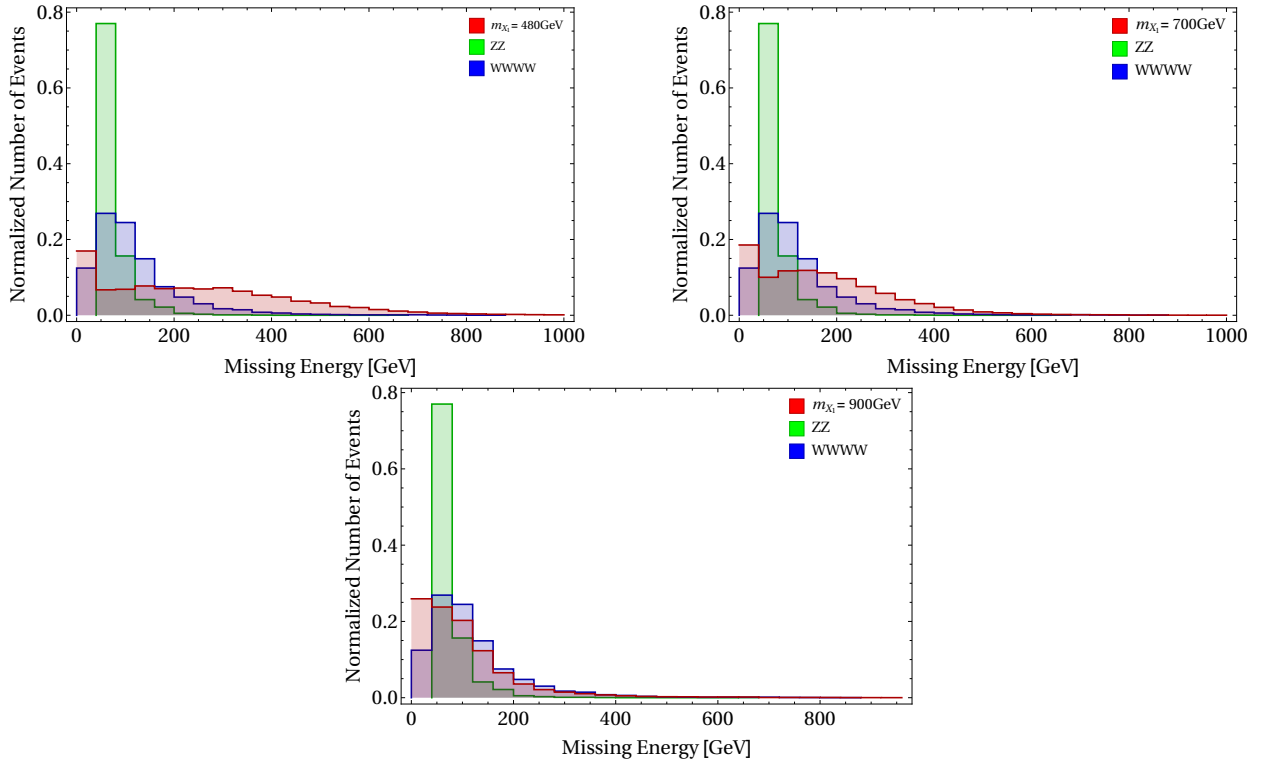


FIG. 28. Missing energy distribution for HQ4l channel for the benchmark points with background events. Top left: BP1, Top right: BP2, Bottom: BP3.

We have also checked the efficiency of invariant mass cut employed in the analysis and explicitly demonstrated that in Fig. 29. In the left panel, we plot invariant mass of opposite sign dilepton in events $\ell^+ \ell^- + 1jet + \cancel{E}_T$ for signal and dominant background from $ZZ + jets$, $WZ + jets$. On the right-panel we plot invariant mass of any two same flavour opposite sign dilepton pair of hadronically quiet four lepton events with dominant SM backgrounds ZZ , $WWWW$. It is evidently visible that the invariant mass for background peaks around m_Z for ZZ and although $WWWW$ peak is understandably more wide, but signal events peak at a larger value. Hence, with a invariant mass cut as performed,

Benchmark Points	$\sigma_{pp \rightarrow X_2 X_2} (in\ pb)$	$\sigma_{pp \rightarrow h_q \bar{h}_q} (in\ pb)$	E_T^{miss}	$\sigma_{pp \rightarrow X_2 X_2}^{HQ4l} (in\ pb)$	$\sigma_{pp \rightarrow h_q \bar{h}_q}^{HQ4l} (in\ pb)$	$N(100fb^{-1})$
BP1	1.93×10^{-2}	1.13	> 100	2.34×10^{-3}	3.39×10^{-4}	267
			> 200	1.92×10^{-3}	1.69×10^{-4}	208
			> 300	1.34×10^{-3}	1.13×10^{-4}	145
BP2	2.64×10^{-2}	7.58×10^{-1}	> 100	2.97×10^{-3}	6.82×10^{-4}	365
			> 200	1.78×10^{-3}	4.16×10^{-4}	219
			> 300	7.45×10^{-4}	7.58×10^{-4}	81
BP3	2.05×10^{-2}	1.02×10^{-1}	> 100	2.93×10^{-4}	1.00×10^{-3}	137
			> 200	5.12×10^{-4}	4.99×10^{-4}	55
			> 300	2.37×10^{-4}	4.48×10^{-4}	47

TABLE IV. Hadronically quiet four lepton ($\ell^+ \ell^- \ell^+ \ell^- + \cancel{E}_T$) events for chosen benchmark points with $p_{T_\ell} > 20$ and $|m_Z - 15| \not\leq m_{ll} \not\leq |m_Z + 15|$ at $\sqrt{s} = 14\ TeV$ and $\mathcal{L} = 100fb^{-1}$ luminosity.

Process	$\sigma_{production} (in\ pb)$	E_T^{miss}	$\sigma_{HQ4l} (in\ pb)$	$N(100fb^{-1})$
ZZ	0.24×10^{-1}	> 100	1.68×10^{-5}	1
		> 200	$< 1.2 \times 10^{-6}$	< 1
		> 300	$< 1.2 \times 10^{-6}$	< 1
$W^+ W^- W^+ W^-$	1.04×10^{-3}	> 100	1.35×10^{-6}	< 1
		> 200	5.2×10^{-8}	< 1
		> 300	5.2×10^{-8}	< 1
$Zt\bar{t}$	0.90	> 100	1.8×10^{-4}	18
		> 200	4.5×10^{-5}	4
		> 300	$< 4.5 \times 10^{-5}$	< 1

TABLE V. HQ4l ($\ell^+ \ell^- + \ell^+ \ell^- + \cancel{E}_T$) events for dominant SM background with $p_{T_\ell} > 20$ and $|m_Z - 15| \not\leq m_{ll} \not\leq |m_Z + 15|$ at $\sqrt{s} = 14\ TeV$ and $\mathcal{L} = 100fb^{-1}$ luminosity. Appropriate K -factors are used for different processes to match to the NLO-NLL cross-sections available in literature (see text for details).

the signal remain unaffected to certain extent while the background drops significantly.

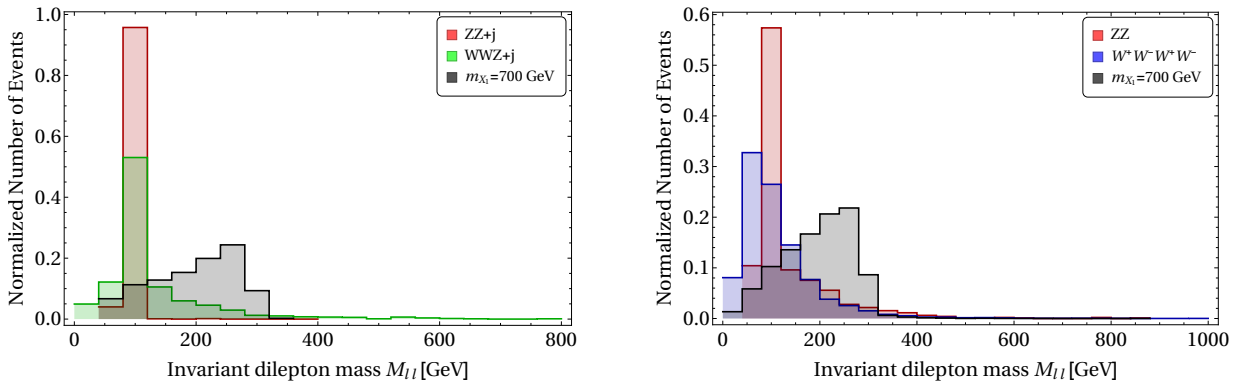


FIG. 29. Invariant mass (m_{ll}) distribution for OSD (left) and HQ4l channel (right) for BP2 compared with Z background.

It is clear that hadronically quiet four lepton channel provides a smoking gun signature of the model as the significance plot suggests in Fig. 30 and it might get unravelled in the early runs of LHC after shut down. It is perhaps possible to look into this channel with the existing data for a possible excess as well. Supersymmetry with R -parity violation can yield signatures of such final states, but doesn't offer a large missing energy as we have here, which helps us to kill the background significantly. On the other hand, supersymmetry in R -parity conserving scenario

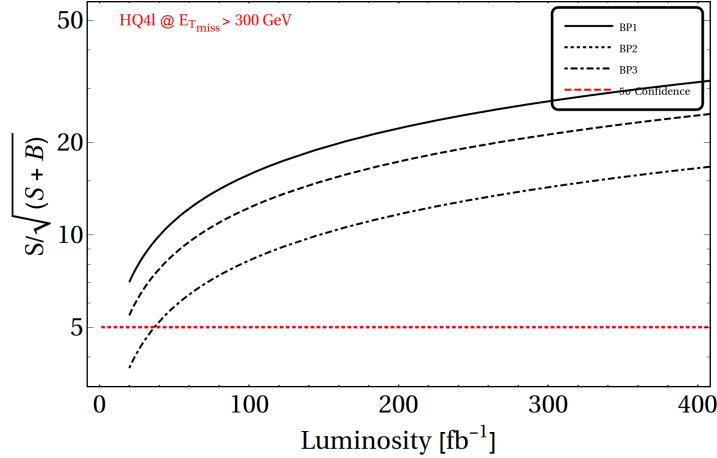


FIG. 30. Significance plot for hadronically quiet four lepton final state for $E_T^{\text{miss}} > 300$ GeV with luminosity.

with light third generation squarks, where gluino decays through stop-top pair yield multi top quarks and hence four lepton final states with large missing energy, but that channel is infected by the presence of multiple b jets. In that sense it is possible to disentangle SUSY from the vector boson dark matter scenario discussed here. Also the existing four lepton search criteria doesn't cater to a large missing energy cut and hence we could not decipher a bound on the X_2 mass from the existing CMS analysis [51]. Here, we may also like to note that four leptons plus two soft jets and missing energy signature arises in our model from the $pp \rightarrow h_q \bar{h}_q$ production and its subsequent decays through heavier gauge bosons exactly in the same way as discussed above. However, the signal cross-section is smaller (for BP1: $\sigma^{4l+2l} = 0.17$ fb with $E_T^{\text{miss}} > 300$ GeV) than the hadronically quiet four lepton events and the background is also larger. Hence, we do not provide a detailed analysis on that.

VI. SUMMARY AND CONCLUSIONS

In this paper we have analysed a dark vector boson model with $SU(2)_N$ extension of SM. We have embedded this in a gauge group $E(6)$, and have shown it is possible to achieve a consistent unification in presence of consistent intermediate symmetries. The breaking adopted here suggests that in D-parity conserved case, $SU(2)_N$ coupling is equal to $SU(2)_L$ coupling ($g_N = g_L$) with two degenerate vector boson DM, but for D-parity broken scenario we may have non-universality through $g_N \neq g_L$ and a single component DM. The spread in the gauge coupling in the latter case is determined by explicit calculation and the freedom is utilised to analyse the DM phenomenology.

One of the crucial construct of the model is to make sure that the $SU(2)_N$ charge do not contribute to hypercharge and therefore having neutral gauge bosons ($X_{1,2,3}$). The stability of the DM (X_1) is achieved by a modified R -charge. Apart from unification, the other important constraint on the model comes from small $X_3 - Z$ mixing. Non-observation of such neutral heavy gauge boson leads to assume $m_{X_3} = m_{Z'} \geq 1$ TeV, which in turn constrains the lower limit of the DM mass for specific g_N . Relic density constraint of the model correlates coupling and mass of the DM to the exotic quark mass m_{h_q} and exotic lepton mass m . Dominant annihilation processes being t channel diagrams through exotic fermion exchange, it allows a large range of DM masses above ~ 200 GeV (with $g_N = g_{2L}$) which is discarded mainly by the vev constraints.

Direct search interaction for this DM is mainly s channel processes and mediates only the exotic quark. Hence excepting for those regions where $m_{h_q} = m_{DM}$, the model is very loosely constrained by spin independent direct search bounds from LUX. Co-annihilation of DM with X_2 can also help the DM to live in even larger region of parameter space and the detection may go beyond the reach of XENON1T sensitivity. This is simply because co-annihilation only contributes to thermal freeze out and hence relic density, but do not take part in direct search reactions. Uncorrelated direct search and relic density is one of the primary outcomes of the analysis and help the DM to live long. We also analysed the degenerate DM scenario in D-parity even case, but there is a conflict between the relic-density and direct search allowed parameter space (where low DM mass is favoured) with the requirement of $m_{X_3} = m_{Z'} \geq 1$ TeV, as three of the gauge bosons including the DM is degenerate in this case. The model also generates neutrino masses but the constraints do not mostly affect the DM phenomenology and hence we do not discuss them in the draft.

While the DM evades the detector, the exotic particle may be produced at LHC and their subsequent decays may

produce interesting multilepton signatures with huge missing energy at LHC. Opposite sign dilepton and hadronically quiet four lepton channels are discussed in this context. Here we note the presence of a soft jet in two lepton signal which helps distinguishing it from SM background events like $t\bar{t}$. Large missing energy cuts are shown to be effective to reduce the background and a possibility of seeing such a signal at 14 TeV LHC emerges. A strong H_T cut as is provided usually in the current analysis of the data washes away the signal cross-section as well. We propose not to use such strong H_T cuts for seeing this signal. The more interesting signal is of course the hadronically quiet four lepton channel, which is a smoking gun signature of such a scenario. SM background for this signal is small, which can be further minimised by employing a high missing energy and invariant mass cut within Z-window. The model can be tested in early runs of LHC at 14 TeV even with a small integrated luminosity. Benchmark points proposed in this draft have been classified according to DM masses with different coupling strength to SM satisfying relic density and direct search constraints. Collider simulations show if an early confirmation of hadronically quiet four lepton channel is not obtained two of our benchmark points (BP1 and BP2) may get ruled out leaving out the option for a heavy vector boson DM. Unlike to most of scalar and fermionic DM scenarios, this model has a stronger constraint from LHC data rather than direct search, although given the existing analysis in these channels, an exact bound on the parameter space was difficult to obtain.

A similar version of the model is available in literature [31] and a comparative analysis will be really helpful to disentangle these frameworks with respect to future observations. Actually a comparative analysis on all possible vector boson DM frameworks should be performed for their relative discovery potential. We will discuss some such possibilities in the next draft.

Acknowledgements: SB would like to acknowledge discussions with Qing-Hong Cao at Argonne National Lab and M. Zakeri of U. C. Riverside; appreciate WHEPP workshop held at IIT Kanpur where part of the work was initiated and acknowledge support from DST INSPIRE faculty award (PHY/P/SUB-01 at IIT Guwahati). BB would like to thank Dr. Subhadeep Mondal of HRI, Allahabad for helping out with the collider simulations, Dr. Flip Tanedo of UC Riverside for his hand written notes on DM direct detection and Prof. Biswarup Mukhopadhyay of HRI, Allahabad for his critical comments on the collider part. BB would also like to acknowledge the hospitality of IIT Kanpur during his visit, where a part of the work was completed. J.C. is supported by the Department of Science and Technology, Government of India, under the Grant IFA12-PH-34 (INSPIRE Faculty Award); and the Science and Engineering Research Board, Government of India, under the agreement SERB/PHY/2016348.

Appendix A: Scalar Potential

The scalar potential of the model is given by :

$$\begin{aligned}
V = & \mu_1^2 \text{Tr} \left(\phi_{13}^\dagger \phi_{13} \right) + \mu_2^2 \left(\phi_2^\dagger \phi_2 \right) + \mu_\chi^2 \left(\chi \chi^\dagger \right) + \mu_\Delta^2 \text{Tr} \left(\Delta^\dagger \Delta \right) + \left(\mu_3^2 \det \Delta + h.c. \right) \\
& + \left(\mu_{22} \tilde{\chi} \phi_{13}^\dagger \tilde{\phi}_2 + \mu_{12} \chi \Delta \tilde{\chi}^\dagger + \mu_{23} \tilde{\chi} \Delta \chi^\dagger + h.c. \right) + \frac{1}{2} \lambda_1 \left(\text{Tr} \left(\phi_{13}^\dagger \phi_{13} \right) \right)^2 \\
& + \frac{1}{2} \lambda_2 \left(\phi_2^\dagger \phi_2 \right)^2 + \frac{1}{2} \lambda_3 \text{Tr} \left(\phi_{13}^\dagger \phi_{13} \phi_{13}^\dagger \phi_{13} \right) + \frac{1}{2} \lambda_4 \left(\chi \chi^\dagger \right)^2 \\
& + \frac{1}{2} \lambda_5 \left[\text{Tr} \left(\Delta^\dagger \Delta \right) \right]^2 + \frac{1}{4} \lambda_6 \text{Tr} \left(\Delta^\dagger \Delta - \Delta \Delta^\dagger \right)^2 + \\
& \tilde{\lambda}_1 \chi \phi_{13}^\dagger \phi_{13} \chi^\dagger + \tilde{\lambda}_2 \chi \tilde{\phi}_{13}^\dagger \tilde{\phi}_{13} \chi^\dagger + \tilde{\lambda}_3 \phi_2^\dagger \phi_{13} \phi_{13}^\dagger \phi_2 + \tilde{\lambda}_4 \phi_2^\dagger \tilde{\phi}_{13} \tilde{\phi}_{13}^\dagger \phi_2 + \\
& \tilde{\lambda}_5 \left(\phi_2^\dagger \phi_2 \right) \left(\chi^\dagger \chi \right) + \tilde{\lambda}_6 \left(\chi \chi^\dagger \right) \text{Tr} \left(\Delta^\dagger \Delta \right) + \tilde{\lambda}_7 \chi \left(\Delta^\dagger \Delta - \Delta \Delta^\dagger \right) \chi^\dagger \\
& + \tilde{\lambda}_8 \left(\phi_2^\dagger \phi_2 \right) \text{Tr} \left(\Delta^\dagger \Delta \right) + \tilde{\lambda}_9 \text{Tr} \left(\phi_{13}^\dagger \phi_{13} \right) \text{Tr} \left(\Delta^\dagger \Delta \right) + \\
& + \tilde{\lambda}_{10} \text{Tr} \left(\phi_{13} \left(\Delta^\dagger \Delta - \Delta \Delta^\dagger \right) \phi_{13}^\dagger \right), \tag{A1}
\end{aligned}$$

where

$$\phi_2 = \begin{pmatrix} \phi_2^+ \\ \phi_2^0 \end{pmatrix}, \quad \tilde{\phi}_2 = \begin{pmatrix} \bar{\phi}_2^0 \\ -\phi_2^- \end{pmatrix}, \quad \phi_{13} = \begin{pmatrix} \phi_1^0 & \phi_3^0 \\ \phi_1^- & \phi_3^- \end{pmatrix}, \quad \tilde{\phi}_{13} = \begin{pmatrix} \phi_3^+ & -\phi_1^+ \\ -\phi_3^0 & \phi_1^0 \end{pmatrix}, \quad \chi = (\chi_1^0 \quad \chi_2^0), \quad \tilde{\chi} = (\bar{\chi}_2^0 \quad -\bar{\chi}_1^0), \tag{A2}$$

and μ_3^2, μ_{23} terms explicitly break L softly to $(-1)^L$.

Appendix B: The Yukawa Couplings

The allowed Yukawa couplings [30] for quarks :

$$(d\phi_1^0 - u\phi_1^-) d^c - (d\phi_3^0 - u\phi_3^-) h_q^c, (u\phi_2^0 - d\phi_2^+) u^c, (h_q^c \chi_2^0 - d_c \chi_1^0) h_q, \tag{B1}$$

For leptons:

$$(N\phi_3^- - \nu\phi_1^- - E\phi_3^0 + e\phi_1^0) e^c, (E\phi_2^+ - N\phi_2^0) n^c - (e\phi_2^+ - \nu\phi_2^0) \nu^c, \tag{B2}$$

$$(EE^c - NN^c) \chi_2^0 - (eE^c - \nu N^c) \chi_1^0, (E^c \phi_1^- - N^c \phi_1^0) n^c - (E^c \phi_2^- - N^c \phi_2^0) \nu^c, \tag{B3}$$

$$n^c n^c \Delta_1^0 + (n^c \nu^c + \nu^c n^c) \Delta_2^0 / \sqrt{2} - \nu^c \nu^c \Delta_3^0. \tag{B4}$$

-
- [1] F.Zwicky, “Spectral displacement of extra galactic nebulae”, *Helv.Phys.Acta* **6**,110 (1933)
- [2] V.Rubin, “Dark matter in spiral galaxies”, *Scientific American* **248**, 96 (1983)
- [3] D. J. Schlegel, D. P. Finkbeiner and M. Davis, *Astrophys. J.* **500** (1998) 525 doi:10.1086/305772 [astro-ph/9710327].
- [4] M. Markevitch *et al.*, *Astrophys. J.* **606** (2004) 819 doi:10.1086/383178 [astro-ph/0309303].

- [5] For a review on Dark Matter, see, for example, G. Bertone, D. Hooper and J. Silk, Phys. Rept. **405**, 279 (2005) doi:10.1016/j.physrep.2004.08.031 [hep-ph/0404175].
- [6] G.Jungman, M. Kamionkowski, K. Griest, Physics Reports **267**(1996) 195-373
- [7] E. W. Kolb and M. S. Turner, Front. Phys. **69**, 1 (1990).
- [8] W. L. Guo and Y. L. Wu, JHEP **1010**, 083 (2010) doi:10.1007/JHEP10(2010)083 [arXiv:1006.2518 [hep-ph]].
- [9] L. Feng, S. Profumo and L. Ubaldi, JHEP **1503**, 045 (2015) doi:10.1007/JHEP03(2015)045 [arXiv:1412.1105 [hep-ph]].
- [10] T. G. Steele, Z. W. Wang, D. Contreras and R. B. Mann, Phys. Rev. Lett. **112**, no. 17, 171602 (2014) doi:10.1103/PhysRevLett.112.171602 [arXiv:1310.1960 [hep-ph]].
- [11] J. M. Cline, K. Kainulainen, P. Scott and C. Weniger, Phys. Rev. D **88**, 055025 (2013) Erratum: [Phys. Rev. D **92**, no. 3, 039906 (2015)] doi:10.1103/PhysRevD.92.039906, 10.1103/PhysRevD.88.055025 [arXiv:1306.4710 [hep-ph]].
- [12] S. Bhattacharya, P. Poulose and P. Ghosh, arXiv:1607.08461 [hep-ph]; S. Bhattacharya, S. Jana and S. Nandi, Phys. Rev. D **95**, no. 5, 055003 (2017) doi:10.1103/PhysRevD.95.055003 [arXiv:1609.03274 [hep-ph]].
- [13] Y. G. Kim, K. Y. Lee and S. Shin, JHEP **0805**, 100 (2008) doi:10.1088/1126-6708/2008/05/100 [arXiv:0803.2932 [hep-ph]].
- [14] N. Okada and T. Yamada, JHEP **1310**, 017 (2013) doi:10.1007/JHEP10(2013)017 [arXiv:1304.2962 [hep-ph]].
- [15] Y. Bai and J. Berger, JHEP **1311**, 171 (2013) doi:10.1007/JHEP11(2013)171 [arXiv:1308.0612 [hep-ph]].
- [16] S. Bhattacharya, N. Sahoo and N. Sahu, Phys. Rev. D **93** (2016) no.11, 115040 doi:10.1103/PhysRevD.93.115040 [arXiv:1510.02760 [hep-ph]].
- [17] S. Bhattacharya, S. Patra, N. Sahoo and N. Sahu, JCAP **1606** (2016) no.06, 010 doi:10.1088/1475-7516/2016/06/010 [arXiv:1601.01569 [hep-ph]].
- [18] S. Bhattacharya, N. Sahoo and N. Sahu, arXiv:1704.03417 [hep-ph].
- [19] S. Bhattacharya, B. Karmakar, N. Sahu and A. Sil, Phys. Rev. D **93** (2016) no.11, 115041 doi:10.1103/PhysRevD.93.115041 [arXiv:1603.04776 [hep-ph]].
- [20] S. Bhattacharya, B. Karmakar, N. Sahu and A. Sil, arXiv:1611.07419 [hep-ph].
- [21] G. Servant and T. M. P. Tait, Nucl. Phys. B **650** (2003) 391 doi:10.1016/S0550-3213(02)01012-X [hep-ph/0206071].
- [22] T. Flacke, D. W. Kang, K. Kong, G. Mohlabeng and S. C. Park, JHEP **1704** (2017) 041 doi:10.1007/JHEP04(2017)041 [arXiv:1702.02949 [hep-ph]].
- [23] A. Datta, U. K. Dey, A. Raychaudhuri and A. Shaw, Phys. Rev. D **88** (2013) 016011 doi:10.1103/PhysRevD.88.016011 [arXiv:1305.4507 [hep-ph]].
- [24] A. Birkedal, A. Noble, M. Perelstein and A. Spray, Phys. Rev. D **74** (2006) 035002 doi:10.1103/PhysRevD.74.035002 [hep-ph/0603077].
- [25] L. Wu, B. Yang and M. Zhang, JHEP **1612** (2016) 152 doi:10.1007/JHEP12(2016)152 [arXiv:1607.06355 [hep-ph]].
- [26] S. Baek, P. Ko, W. I. Park and E. Senaha, PoS DSU **2012**, 010 (2012) [arXiv:1301.1773 [hep-ph]].
- [27] M. Duch, B. Grzadkowski and M. McGarrie, JHEP **1509** (2015) 162 doi:10.1007/JHEP09(2015)162 [arXiv:1506.08805 [hep-ph]].
- [28] Y. Farzan and A. R. Akbarieh, Phys. Lett. B **724**, 84 (2013) doi:10.1016/j.physletb.2013.06.004 [arXiv:1211.4685 [hep-ph]].
- [29] J. L. Diaz-Cruz and E. Ma, Phys. Lett. B **695**, 264 (2011) doi:10.1016/j.physletb.2010.11.039 [arXiv:1007.2631 [hep-ph]].
- [30] S. Bhattacharya, J. L. Diaz-Cruz, E. Ma and D. Wegman, Phys. Rev. D **85**, 055008 (2012) doi:10.1103/PhysRevD.85.055008 [arXiv:1107.2093 [hep-ph]].

- [31] S. Fraser, E. Ma and M. Zakeri, Int. J. Mod. Phys. A **30**, no. 03, 1550018 (2015) doi:10.1142/S0217751X15500189 [arXiv:1409.1162 [hep-ph]].
- [32] S. M. Boucenna, M. B. Krauss and E. Nardi, Phys. Lett. B **755** (2016) 168 doi:10.1016/j.physletb.2016.02.008 [arXiv:1511.02524 [hep-ph]].
- [33] N. Nagata, K. A. Olive and J. Zheng, JHEP **1510** (2015) 193 doi:10.1007/JHEP10(2015)193 [arXiv:1509.00809 [hep-ph]].
- [34] G. Hinshaw *et al.* Nine-year Wilkinson Microwave Anisotropy Probe (WMAP) Observations: Cosmological Parameter Results [arXiv: 1212.5226]
- [35] P. A. R. Ade *et al.* [Planck Collaboration], Astron. Astrophys. **594**, A13 (2016) doi:10.1051/0004-6361/201525830 [arXiv:1502.01589 [astro-ph.CO]].
- [36] D. S. Akerib *et al.* [LUX Collaboration], Phys. Rev. Lett. **118**, no. 2, 021303 (2017) doi:10.1103/PhysRevLett.118.021303 [arXiv:1608.07648 [astro-ph.CO]].
- [37] G. C. Branco, P. M. Ferreira, L. Lavoura, M. N. Rebelo, M. Sher and J. P. Silva, Phys. Rept. **516**, 1 (2012) doi:10.1016/j.physrep.2012.02.002 [arXiv:1106.0034 [hep-ph]].
- [38] G. Bhattacharyya and D. Das, Pramana **87**, no. 3, 40 (2016) doi:10.1007/s12043-016-1252-4 [arXiv:1507.06424 [hep-ph]].
- [39] V. V. Andreev, P. Osland and A. A. Pankov, Phys. Rev. D **90**, no. 5, 055025 (2014) doi:10.1103/PhysRevD.90.055025 [arXiv:1406.6776 [hep-ph]].
- [40] A. Flrez, A. Gurrola, W. Johns, Y. D. Oh, P. Sheldon, D. Teague and T. Weiler, Phys. Lett. B **767** (2017) 126 doi:10.1016/j.physletb.2017.01.062 [arXiv:1609.09765 [hep-ph]].
- [41] Michael E. Peskin, Daniel V. Schroeder: An Introduction to Quantum Field Theory.
- [42] Paolo Gondolo, Graciela Gelmini Cosmic Abundances of Stable Particles: Improved Analysis Nuclear Physics **B 360** (1991) 145-179.
- [43] J. Hisano, K. Ishiwata, N. Nagata and M. Yamanaka, Prog. Theor. Phys. **126**, 435 (2011) doi:10.1143/PTP.126.435 [arXiv:1012.5455 [hep-ph]].
- [44] J. Hisano, R. Nagai and N. Nagata, JHEP **1505**, 037 (2015) doi:10.1007/JHEP05(2015)037 [arXiv:1502.02244 [hep-ph]].
- [45] J. Chakraborty and A. Raychaudhuri, Phys. Rev. D **81**, 055004 (2010) doi:10.1103/PhysRevD.81.055004 [arXiv:0909.3905 [hep-ph]].
- [46] A. Belyaev, N. D. Christensen and A. Pukhov, Comput. Phys. Commun. **184**, 1729 (2013) doi:10.1016/j.cpc.2013.01.014 [arXiv:1207.6082 [hep-ph]].
- [47] T. Sjostrand, S. Mrenna and P. Z. Skands, JHEP **0605**, 026 (2006) doi:10.1088/1126-6708/2006/05/026 [hep-ph/0603175].
- [48] R. Placakyte, arXiv:1111.5452 [hep-ph].
- [49] J. Alwall *et al.*, JHEP **1407** (2014) 079 doi:10.1007/JHEP07(2014)079 [arXiv:1405.0301 [hep-ph]].
- [50] CMS Physics Analysis Summary, Search for new physics in final states with two opposite-sign same-flavor leptons, jets and E_T^{miss} in pp collisions at $\sqrt{s} = 13$ TeV **CMS PAS SUS-16-011**
- [51] CMS Physics Analysis Summary, Search for SUSY with multileptons in proton proton collisions at $\sqrt{s} = 13$ TeV **CMS PAS SUS-16-003**
- [52] M. Aaboud *et al.* [ATLAS Collaboration], arXiv:1611.05791 [hep-ex].